International Journal of
Turbomachinery Propulsion and Power

MDPI

Article

A Reliable Update of the Ainley and Mathieson Profile and Secondary Correlations

Yumin Liu [1,*], Patrick Hendrick [1], Zhengping Zou [2] and Frank Buysschaert [3]

1 Department of Aero-Thermo-Mechanics, Université Libre de Bruxelles, 1050 Brussels, Belgium; patrick.hendrick@ulb.be
2 School of Energy & Propulsion Engineering, Beihang University, Beijing 100191, China; zouzhengping@buaa.edu.cn
3 Department of Applied Mechanics & Energy Conversion, Katholieke Universiteit Leuven, 8200 Brugge, Belgium; frank.buysschaert@kuleuven.be
* Correspondence: yu.m.liu@ulb.be

Abstract: Empirical correlations are still fundamental in the modern design paradigm of axial turbines. Among these, the prominent Ainley and Mathieson correlation (Ainley D. and Mathieson G., 1951, "A Method of Performance Estimation for Axial-Flow Turbines," ARC Reports and Memoranda No. 2974) and its derivatives, plays a crucial role. In this paper, the underlying assumptions of the aforementioned models are discussed by means of a descriptive review, whilst an attempt is made to enhance their reliability and, potentially, accuracy in performance estimations. Closer investigation reveals an intriguing misuse of the lift coefficient in the secondary loss. In light of this, an enhanced model that, notably, builds upon the Zweifel criterion and the vortex penetration depth concept is developed and discussed. The obtained accuracy is subsequently assessed through CFD computations, employing a database comprising 109 cascades. The results indicate a 50% probability of achieving the ±15% error interval, which is twice as good as the most recent Aungier model (Aungier R., 2006, "Turbine Aerodynamics: Axial-Flow and Radial-Inflow Turbine Design and Analysis", ASME Press, New York). Furthermore, the reliability of the proposed model is demonstrated by a reconstruction of the Smith chart, on the one hand, and a performance analysis, on the other. The reconstruction exhibits contours that conform to the original. The results of the performance study are compared with the CFD solutions of eight cascades working in off design conditions and confirm the need of the additionally included turbine design parameters, such as the axial velocity and the meanline radius ratios.

Keywords: loss correlation; axial-flow turbine; turbine performance

Citation: Liu, Y.; Hendrick, P.; Zou, Z.; Buysschaert, F. A Reliable Update of the Ainley and Mathieson Profile and Secondary Correlations. *Int. J. Turbomach. Propuls. Power* **2022**, 7, 14. https://doi.org/10.3390/ijtpp7020014

Received: 2 December 2021
Accepted: 3 April 2022
Published: 21 April 2022

1. Introduction

The axial turbine became incontestably the accustomed device for medium to high mechanical power generation in modern powerplants and therefore, not surprisingly, it still remains the subject of extensive research. Throughout the past decades, experience and knowledge have grown continuously, adding refinements to the art of turbine design. In this study, the 1D aerodynamic design, more specifically, the loss correlations employed in the meanline analysis used in the early design phase, are reviewed. These models are crucial, as they set the preliminary design parameters that can be maintained up to the final design stage, that is, if the model incorporates sufficient levels of reliability [1]. Among these, it is evident to note the renown Ainley and Mathieson (AM) correlation, published in 1957, which serves this purpose [2] well. For the record, Ainley and Mathieson's model was considered to be a significant innovation, as it enabled the quantification of local losses. It was, e.g., successfully employed in the design process of the Rolls Royce Olympus engine [3]. Being the cradle leading to great successes and broad acceptance, it underwent multiple updates [4–6], which expanded into a veritable genealogy.

Over time, the design of axial turbines underwent several improvements and the geometry became much more diverse, causing the accuracy and reliability of the current historic correlation based (open source) 1D models to become less effective. An important issue is their mathematical foundation, which relies on a fuzzy blend of classical flow theory and heuristic manipulations matching the early cascade measurements [7]. Hence, it is not surprising that modern turbines may become excluded from their range of application. In light of this, studies have evaluated the correlation reliability through parametric analysis [8–10]. Although inconsistencies have been identified and reported, no remedies have been proposed. Accuracy has been evaluated on few test cases, which is insufficient to affirm any statistical significance. These two aspects (reliability and accuracy) have to be investigated with statistical evidence to clarify the true potential of the available 1D correlations with the latest turbines. Moreover, it is deemed mandatory to upgrade the correlations with a more robust physics based backbone, compatible with modern turbines.

The objective of this paper is, therefore, twofold. The first is to provide a comprehensive review of the AM family correlations. The second is to enhance the AM correlation based on recent breakthroughs in turbine aerodynamics and loss mechanisms, and boosting compatibility with current design workflows. In particular, the Zweifel criterion [11] and the depth penetration [12,13] are integrated into the latest Aungier (Ag) profile and secondary loss models [6]. The latter are validated on a data set composed of 109 cascades (static and rotating) to achieve statistical significance in terms of accuracy and reliability. High fidelity simulations and their numerical solutions serve as the benchmark during the evaluations. The correlation accuracy is determined in terms of probability according to the Gaussian distribution of the relative errors, whilst the correlation reliability is proven by its ability to reproduce the Smith chart [14] and maintain consistent trends in off design conditions under the variation of the newly introduced axial velocity ratio.

2. Review

The importance of empirical loss correlations still remains high in the design process of modern axial turbines. Despite their restricted fidelity, they can effectively offer guidance in decision making during the preliminary design stages [1]. In general, the development of empirical models is built upon on a turbine database, which is produced by means of experimental tests where a multitude of measurements are performed and linked to several, mostly dimensionless, design parameters. When parameters are found to correlate well, dedicated design laws can consequently be established.

Quite recently, there was a spirited debate on the capability of cascade tests to approximate real turbine flow. The proponents claimed that cascades could offer a satisfactory basis for estimating losses in real machines and should be preferred thanks to their simplicity, flexibility and low cost [15]. The opponents, however, believe that cascades are inherently limited since they cannot reproduce key aspects of the real operation environment, involving, e.g., rotational, curvature and inlet flow distortion effects [16]. Despite this contention, the current state of the art research has clearly joined the supporting side, considering the solid foothold of cascade tests in public literature. The authors of this work adhere to the standpoint of Craig and Cox (CC) [17], which holds a certain relativism. In fact, the extreme situation in which application of the correlations fails in both accuracy and reliability is rather unlikely. However, careless use must be avoided, as this could lead to an entirely erroneous result [18,19]. Hence, the user has to be fully aware of the features and limitations involved, so that the correlations can be applied effectively in real turbine design. This aspect is the crux of the following discussions.

Correlations are typically determined by the investigator's own judgment, experience and interpretation of flow physics, test quality and database size [20]. The challenge resides in the way the wide information of a complex 3D flow is filtered and condensed into a 1D empirical model. During its setup, certain parameters could be deliberately biased, with the objective to reflect specific turbine characteristics. The reason behind this intervention is quite straightforward. For example, aero-engine and land based steam turbines do not share the same design requirements, as is the case with high and low pressure turbines. They differ by design and aerodynamics and so will the correlations. The comparative studies of several public domain correlations [9,21] emphasized this issue clearly. As a consequence, there are no universal turbine correlations at this point. Hence, they only serve a specific range of applications adequately.

Since it is common to use empirical models for a wide range of turbine design applications, it is not surprising that the parameters estimated from the cascade correlation may disagree with real machine measurements by a considerable order of magnitude. In these circumstances, one resorts typically to a heuristic calibration. Otherwise, the correlation is of little value [22]. However, there are some risks involved with such an approach. First, simple multipliers/polynomials are often deemed sufficient, even though the resulting correlation would much better suit turbines akin to those used in the database from which the model was established. Second, its use inherently leads to designs whose aerodynamics are similar to that of the turbines in its original database. The fundamental issue is the statistical bias engendered by the limited size of the database. This could be prevented by the construction of a large public database collecting all cascade measurements performed up to the present day [7]. Unfortunately, early investigators did not share or even lost their databases. New investigators often had to generate a new database from the ground up, with neither access to previous data, nor methodologies. In particular, insights that could have revealed a stronger interaction between design parameters, were curtailed. As a consequence, 1D correlations revert to quite simple mathematics or charts and are biased, which, thus, leads to results with rather low fidelity. In contrast, the models established in large industries do not suffer from the aforementioned issues, where one can afford the calibration of public domain or in-house correlations using the vast amount of data accumulated over time for dedicated configurations. From this data, new versions of earlier models can be developed, which enables a safer and cheaper enhancement of the design process.

In [23], it was advanced that any loss correlation exhibits the same probability to accurately predict turbine performance once out of its range of application. Considering the current discussion, it is rather irrational to expect outstanding accuracy from models that attempt to cover complex systems with elemental information. With full awareness of the higher fidelity 3D methods intervening at later design stages, correlation accuracy should be less prioritized, but the focus must initially go towards including all relevant design parameters in the model. Therefore, the ability to cope coherently with the true physics, i.e., reliability, must become the primary concern.

2.1. Ainley and Mathieson Family Correlations

The empirical AM correlation [2] has been so successful that it owns a lineage (the AM correlation and its derivatives will not be differentiated in this framework, as these are fundamentally equivalent). Chronologically, it was established through cascade tests using conventional profiles stemming from the 1940s and claimed a nominal accuracy of $\pm 2\%$ in stage efficiency estimation. The latter corresponds to about $\pm 15\%$ total pressure loss error. It was published at a time when the expertise and the understanding of axial compressors were more profound than those of turbines [24]. As a matter of fact, before AM was published, one had to resort to expensive experimental trial and error processes when the available methods revealed efficiencies largely inferior to those of the actual turbines. The AM correlation was, therefore, considered to be groundbreaking, as it provides a systematic way to quantify turbine aerodynamic loss and its components.

The Dunham and Came (DC) correlation [4] was the first and a canonical update to the model of AM, which used 16 1960s technology Rolls Royce turbines. It extended the application range to small turbines, while retaining the same accuracy level. Dunham claimed that their model was still the most reliable design tool during the 1970s, in a context where there was a progressive adoption of potential flow calculation in industry [3]. However, the investigators did not have access to the database of AM and, thus, the improvement resulted from model calibration based on the overall performance of a restricted number of turbines. It is noteworthy to mention that CC [17], along with Traupel [25], published new correlations with different approaches with regard to turbine aerodynamics in that same period. The Kacker and Okapuu (KO) correlation [5] came as a second update based on 33 1980s technology Pratt & Whitney turbines and showed an accuracy up to $\pm 1.5\%$ in stage efficiency estimation in design conditions. Furthermore, KO, having high confidence in the validity of the Smith chart [14] which contains 70 1960s technology Rolls Royce turbines [26], calibrated their correlation to fittingly reproduce the same chart. Ag [6] subsequently revised KO to handle recompression produced in extreme off design conditions and real working fluids. In addition, it can cope with hub to shroud S2 calculations (the hub to shroud S2 and blade to blade S1 calculations proposed by Wu [27] refer to stream surfaces on which 2D flow equations are solved by mass-averaging the third coordinate). This has recently been confirmed, notably in ORC turbines [28,29]. Despite many the critics of its limitations, the choice of the AM correlation over other public correlations is driven by three particular aspects. Firstly, it owns a comparatively broader mathematical basis and is less reliant on empirical charts. Secondly, it does not require specific assumptions on the blade surface velocity distribution nor the need to perform cumbersome mathematical computations. As a consequence, faster solution and better accessibility are ensured, in contrast to the semi-empirical models of Baljé and Binsley [30], Denton [31] and Coull and Hodson [32]. Lastly, transparent and valuable details of its development can be retraced in the successive works [2,24,33,34].

There are five sources of total pressure loss encountered in aerodynamics, notably, skin friction, pressure drag, shock, leakage and mixing losses. However, this classification was rearranged to associate these losses to their location instead of their phenomenological origin. The AM family correlations assumed the turbine loss system as follows:

$$\begin{aligned} Y_t &= \frac{p_{tr,out,is} - p_{tr,out}}{p_{tr,out} - p_{out}}, \\ &= Y_p + Y_s + Y_{cl}. \end{aligned} \tag{1}$$

- Profile loss Y_p is generated by the growth of the boundary layer and flow mixing over the blade surface. This encompasses skin friction and pressure drag. In case the exit flow reaches supersonic velocities and triggers shocks near the trailing edge, then an additional supersonic loss Y_{ex} is to be accounted for. These losses exclusively arise from blade to blade S1 flow and thus assume spanwise uniformity.
- Secondary loss Y_s originates from the interaction between endwall flow and the pressure difference across the blade passage. The main actors are the 3D induced vortices and endwall boundary layers. AM, drawing on the model of Carter [35], regarded both flows and the annulus loss as one entity. This local loss is responsible for spanwise non-uniformity at blade tip and hub.
- Tip leakage loss Y_{cl} arises from the presence of a gap between the blade tip and the shroud, preventing the rotating blade from rubbing against the casing. Although this is indispensable to complete the loss system, this loss is not considered within the scope of this work, where priority is given to the more fundamental profile and secondary losses.

Although it was not specified, the correlations implicitly refer to losses of fully mixed flow. However, to be precise, there is neither theoretical nor experimental evidence that can justify the breakdown of Equation (1), as this inherently assumes little interaction between the components [36]. However, its effectiveness might be due to the comparatively small chord of axial turbine blades and the short flow transit time in the blade passage inhibiting strong interaction between the secondary flows (all flows that differ from the primary inviscid flow) [7].

2.2. Profile Losses

The AM 2D profile loss [37] is

$$Y_{p,AM} = \left[Y_{p,\theta_{in}=0^\circ} - \left| \frac{\theta_{in}}{\beta_{out}} \right| \left(\frac{\theta_{in}}{\beta_{out}} \right) \left(Y_{p,\theta_{in}=-\beta_{out}} - Y_{p,\theta_{in}=0^\circ} \right) \right] \left(\frac{5t_{max}}{c} \right)^{-K_m \frac{\theta_{in}}{\beta_{out}}}, \\ = f(s/c, t_{max}/c, \theta_{in}, \beta_{out}). \quad (2)$$

AM blended the profile losses of a slightly compressible 50% reaction nozzle $Y_{p,\theta_{in}=0^\circ}$ and impulse nozzle $Y_{p,\theta_{in}=-\beta_{out}}$, as depicted in their Figure 4 on page 24 in [2], to cover all intermediate designs. This correlation inherently comprises the trailing edge loss taken at standard $t_{te}/s = 0.02$. Equation (2) was obtained from low speed wind tunnel tests and focuses on parabolically cambered conventional profiles, i.e., the British T.6 type profiles. Their experimental results showed the notable sensitivity of the losses to the profile thickness in impulse profiles and, thus, a correction for any deviation from standard $t_{max}/c = 0.2$ [34] was introduced in the model. In addition, there was a variation according to $(\theta_{in}/\beta_{out})^2$ for profiles in-between the impulse and nozzle blades, hence justifying the arrangement/blending in Equation (2). The velocity distribution of the nozzle and impulse blades was presented in AM's Figure 5 on page 26 in [34]. This distribution shows that a considerable portion of the suction side of the blade extending from midchord to trailing edge is affected by flow diffusion, which is nowadays regarded as unacceptable in design standards. Use of AM would, therefore, implicitly assume a similar velocity distribution over modern turbine profiles, which is likely to result in a significant loss mismatch if not handled with care [38]. This specific problem with associated implications has to be addressed when enhancing Equation (2).

In order to improve the reliability of the model of AM for recent turbine configurations, several correction factors—in this work designated as the auxiliary factors$K$—have been proposed by different authors [4,5]. For example, in his latest update, Ag [6] adapted the profile loss correlation of KO (and, thus, AM). This equation possesses several auxiliary factors and is expressed as:

$$Y_{p,Ag} = K_{mod} K_M K_p K_{Re} \left(K_i Y_{p,AM} - Y_{t_{te}=0.02s} \right) + Y_{sh}, \\ = f(e_c/s, \theta_{in}, \theta_{out}, M_{r,in}, M_{r,out}, Re, e/c, k, i) Y_{p,AM}. \quad (3)$$

- Mach correction factor $K_p \leq 1$ reflects the flow acceleration in the blade passage reducing viscous loss and acts in the subsonic range $M_{r,out} \geq 1$. According to Ag [6], K_p, introduced for the first time by KO, is flawed in extreme off-design conditions, especially when recompression occurs at the blade hub. It was known that KO yielded only satisfactory results at the design point [15]. Wei [9] tested KO and exposed a curious slope disruption and a nonphysical reduction in the predicted profile losses in cases of higher positive incidences i resulting in recompression, because of spurious K_p values. It is also noteworthy that the impact of the Mach number was investigated by AM [24] and is consistent with the purpose of K_p, but it was, surprisingly, not adopted in the earlier Equation (2).
- Expansion correction factor $K_M \geq 1$ deals with local weak shocks on the blade suction side in the subsonic exit Mach number band $M_{r,out} \in [0.6–1]$ and was rendered more physics driven. This parameter was first introduced by DC [4] for supersonic flows and was derived from the overall turbine performance established by means of experiments.
- Reynolds correction factor K_{Re} applies to Reynolds numbers outside the transition range $[10^5–5 \times 10^5]$ and includes surface roughness, as seen in the CC correlation [17]. A standard finish of $e/c = 10^{-4}$ is assumed throughout the analysis.
- Technology correction factor K_{mod} copes with the technology mismatch of $Y_{p,AM}$ when examining the losses in post-1980s turbine profiles [37]. K_{mod} takes the value of 0.825 for meridional entry profiles and 2/3 for the other.

- Incidence correction factor $K_i \geq 1$ conditions the profile loss in off design conditions and was proven to be successful in pre-1980s turbines [39] but overly conservative in modern turbines [15].

In summary, the purpose of the auxiliary factors is to calibrate Equation (2) with its underlying velocity distribution, without the need for an in depth understanding or elaboration of the loss mechanisms. This is evidently caused by a lack of knowledge transfer between AM, DC, KO and Ag [7]. The shock factor $Y_{sh} \geq 0$ accounts for local shocks situated on hub profiles with a thicker leading edge under comparatively high inlet velocities and is exclusively considered as an independent loss contributing to the profile loss, as introduced by KO. However unlike that of KO, it is unaffected by the auxiliary factors. If $M_{r,out} \geq 1$, then K_p and K_M are held at $M_{r,out} = 1$ and the supersonic loss Y_{ex} has to be supplemented to Y_p in Equation (3). Ag proposed

$$Y_{ex,Ag} = \left(\frac{M_{r,out} - 1}{M_{r,out}}\right)^2. \tag{4}$$

It must be recognized that this is a rather arbitrary formulation. However, this is retained throughout the analysis because there are no more reliable alternatives at the moment.

As mentioned earlier, Equation (2) encompasses the trailing edge loss for standard $t_{te}/s = 0.02$. For any variation of t_{te}/s, AM proposed a trailing edge correction factor affected to Equation (1), such that

$$Y_t = K_{te}(Y_p + Y_s + Y_{cl}). \tag{5}$$

This expression interrelates the trailing edge to the profile, and secondary and tip clearance losses and was criticized by KO for its weak physical soundness regarding the latter two options. In fact, neither of the endwall nor tip leakage vortices remain closely attached to the blade surface upon reaching the blade exit, rendering interaction between the vortices and the trailing edge wake flow unlikely. Instead, KO employed a more intuitive approach and proposed the trailing edge loss Y_{te} as an independent component [5], such that

$$Y_t = Y_p + Y_s + Y_{cl} + Y_{te}. \tag{6}$$

However, Y_{te} still remains part of Y_p in a broader sense, so that Equation (1) is not contracted. To enable this expression, one has to virtually bring Equation (2) to $t_{te}/s = 0$ beforehand. However, Ag carried on this approach and formulated the trailing edge loss as the consequence of an abrupt area enlargement:

$$Y_{te,Ag} = \left(\frac{t_{te}}{o - t_{te}}\right)^2. \tag{7}$$

Correction to zero of the trailing edge of Equation (2) is performed by the subtraction of $Y_{t_{te}=0.02s}$.

2.3. Secondary Losses

The AM 3D gross secondary loss is presented by the following equation [2]:

$$\begin{aligned} Y_{s,AM} &= \lambda_{AM} Z, \\ &= f(\beta_{in}, \beta_{out}, \theta_{in}, A_{out}/A_{in}, r_{hub}/r_{tip}). \end{aligned} \tag{8}$$

This compact expression was the result of continuous efforts to interpret turbine endwall secondary flows. λ_{AM} and Z are intrinsic parameters of the AM correlations and originate from the work of Carter [35], who drew on the classical secondary flow theory. The intent of AM was to define a common and unique basis between axial compressors and turbines to quantify secondary losses, as one had (historically) the objective to employ mostly similar blades for both devices. The theory associates endwall vortices with passage vortices produced in curved channels [40]. The latter originate from the distortion of the inlet endwall boundary layer by the near-wall velocity deficit and the blade passage pressure gradient, causing the inception of a helical cross-flow motion spreading throughout the blade passage, as shown in Figure 1a.

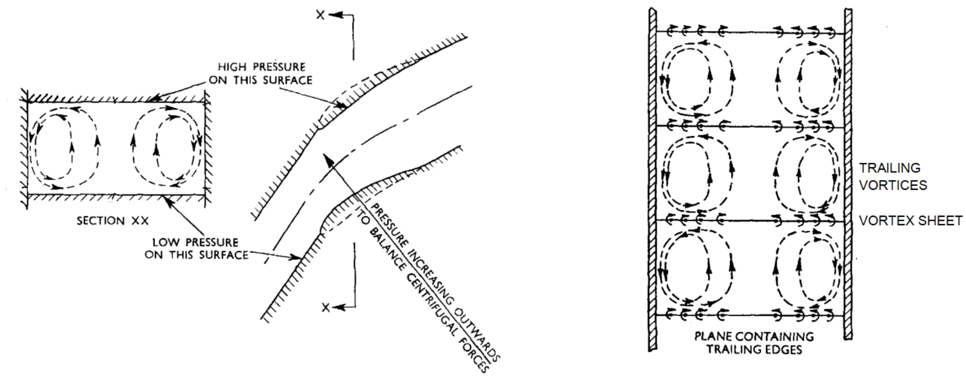

(**a**) (**b**)

Figure 1. Secondary flow mechanisms considered by Carter [35]. (**a**) Classical secondary flow model. (**b**) Cascade lifting line model.

As Carter strived for a practical model to quantify the losses incurred by these passage vortices, he made an analogy with the lifting line theory to obtain a first order approximation. The idea that Carter used leans on the trailing edge inviscid vortex sheet produced by flow circulating around a blade. Being unstable, the closed vortex filaments of the vortex sheet roll up into trailing vortices at the blade ends, as shown in Figure 1b. Based on qualitative analyses of some experimental evidence taken downstream of the blade, the modelled trailing and passage vortices were made equivalent, to establish a secondary loss correlation [35]. Hence, the induced drag under uniform spanwise circulation is:

$$C_{D,s} = \frac{1}{4}\frac{C_{L,m}^2}{s/c}\left(1 - \frac{2H'}{H}\right) = \lambda_{AM}\frac{C_{L,m}^2}{s/c}, \tag{9}$$

with H' the distance from blade midspan to the core of the endwall vortices. This loss coherently reflects lost work by the product of blade loading and the width of the trailing vortices; an analogy to force time displacement. AM subsequently replaced H' by the empirical *Ainley parameter* λ_{AM}, which is shown in their Figure 16 on page 31 in [34], and which reflects the vortex characteristics implicitly. The involved lift coefficient $C_{L,m}$ refers to the mean velocity and relates to the mean angle β_m, where

$$C_{L,m} = 2\frac{s}{c}(\tan\beta_{in} - \tan\beta_{out})\cos\beta_m, \tag{10}$$

and

$$\beta_m = \tan^{-1}\left(\frac{\tan\beta_{in} + \tan\beta_{out}}{2}\right). \tag{11}$$

This was transformed into the *Ainley loading* Z with:

$$Y_{s,AM} = C_{D,s}(\cos^2\beta_{out}/\cos^3\beta_m)(c/s) = \lambda_{AM}Z, \tag{12}$$

where:

$$Z = \frac{C_{L,m}^2}{s/c}\frac{\cos^2\beta_{out}}{\cos^3\beta_m}\frac{c}{s} = 4(\tan\beta_{in} - \tan\beta_{out})^2\frac{\cos^2\beta_{out}}{\cos\beta_m}. \tag{13}$$

This equation assumes an axial velocity ratio AVR and meanline radius ratio κ, with: $\mathrm{AVR} = W_{z,out}/W_{z,in} = \kappa = r_{in}/r_{out} = 1$ and is fully independent of s/c. Note that a change in blade loading due to a pitch to chord variation would not be identifiable [41]. As a matter of fact, this expression is much closer to the lift coefficient of a single airfoil. The chosen lifting line theory is also used under steady and incompressible conditions and is applied to low camber/loading blades to guarantee the linearity of the problem. As a result, a large disagreement in secondary loss may arise in impulse turbine blades [8] and Equation (13) may wrongfully override other parameters under high loadings [10]. AM were aware of this issue, given the shortage of high-loading blades in their database [34].

It is also interesting to note that a mathematical "mistake" occurred with respect to Equation (12). Normally, the outcome should have been [40]:

$$Y_{s,AM} = C_{D,s}(1/\cos\beta_m)(c/s), \tag{14}$$

and consequently, Equation (13):

$$Z = 4(\tan\beta_{in} - \tan\beta_{out})^2 \cos\beta_m \tag{15}$$

which yields results that are several orders of magnitude higher. This indicates that Equation (12) was most likely adapted heuristically to match the measurements. Therefore, as they possess little physical meaning, λ_{AM} and Z cannot be taken apart in the analysis [7]. This is not surprising, since the secondary loss of AM in Equation (8) was calibrated with:

$$Y_s = Y_t - Y_p \tag{16}$$

This corresponds to Equation (1) in absence of clearance losses but has another implication. In fact, the secondary loss was calibrated to the subtraction of the measured true total loss by the modelled profile loss of Equation (2). Hence, Equation (8) embodies the errors associated to Equation (2). As is the case with λ_{AM} and Z, secondary and profile losses should also not be used separately, as they are bound together by Equation (16).

Dunham [19] criticized the approach of Carter but still relied on it to produce

$$\begin{aligned} Y_{s,AMDC} &= 0.0334 K_{AR}\left(\frac{\cos\beta_{out}}{\cos\theta_{in}}\right)Z, \\ &= f(H/c, \beta_{in}, \beta_{out}, \theta_{in}). \end{aligned} \tag{17}$$

The aspect ratio factor $K_{AR} \geq 1$ relates the intensity of the endwall vortices with blade height and was reported to have questionable reliability [42]. DC simplified the multipliers in Equation (13) using a cascade configuration

$$\lambda_{AM} = f\left(\frac{(A_{n,out}\cos\beta_{out}/A_{n,in}\cos\theta_{in})^2}{(1+d_{hub}/d_{tip})}\right) = f\left(\frac{1}{2}\left(\frac{\cos\beta_{out}}{\cos\theta_{in}}\right)^2\right) = 0.0334 K_{AR}\left(\frac{\cos\beta_{out}}{\cos\theta_{in}}\right) \tag{18}$$

The constant 0.0334 is expected to cover most inlet boundary layer thicknesses and was obtained by calibration to overall turbine performance data [22]. Even though this crude approach is not able to estimate the downstream endwall loss of cascade flows [18], it was, however, proven to be more accurate than most refined correlations tested and compared under diverse inlet boundary layer profiles [43]. Eventually, Ag improved Equation (17) to

$$\begin{aligned} Y_{s,Ag} &= K_p K_{Re}\left(\frac{Y_{s,AMDC}^2}{1+7.5Y_{s,AMDC}^2}\right)^{\frac{1}{2}}, \\ &= f(M_{r,in}, M_{r,out}, Re, e/c) Y_{s,AMDC}, \end{aligned} \tag{19}$$

which shares the K_p and K_{Re} of Equation (3) [6]. Nevertheless, K_{Re} was inherited from DC and was later removed by KO. They certainly did not agree on the impact of viscosity on the endwall flow and, interestingly, the debate is still ongoing. It is true that the endwall vortices are mostly driven by inviscid mechanisms. However, their growth in the blade passage highly depends on the endwall boundary layer flow preceding the blade leading edge and continuous interaction with the blade surface boundary layer. Thereby, the approach of DC and Ag is more plausible. The square root manipulation prevents loss overshoots in extreme off design conditions. This feature has proven to be particularly crucial in optimization. In fact, the search algorithm could inadvertently exploit inconsistencies of the correlation to reach its objective [44].

Again, the auxiliary factors act as moderate multipliers to the basic Equation (17). It is interesting to note that the aptness of the axial turbine loss correlations was investigated in the context of centrifugal turbines, and, more specifically, the interaction of the auxiliary factors [23]. Drastic changes in the aerodynamic parameters did not trigger a comparable variation in the auxiliary factors, which could have guaranteed reliable solutions. Hence, these auxiliary factors can only sustain minor and individual adjustment and, thus, axial turbine correlation should only be used with axial turbines.

3. Profile Loss Enhancement

The Ag correlation [6], being the latest complete loss system, constitutes the most suitable vessel for successive enhancements. Thus, the profile loss of Equation (3) is revamped into

$$\begin{aligned} Y_{p,Enh} &= 0.914 K_{mod} K_M K_p K_{Re} Y_{p,AM} + Y_{sh} + Y_{inc}, \\ &= f(e_c/s, \theta_{in}, \theta_{out}, M_{r,in}, M_{r,out}, Re_s, e/c, k, i, d_{LE}/s, We_{LE}, \mathrm{AVR}) Y_{p,AM}, \end{aligned} \tag{20}$$

in which Equation (2) is rewritten as

$$\begin{aligned} Y_{p,AM} &= \left[Y_{p,\beta_{in}=0^\circ} - \left| \frac{\beta_{in}}{\beta_{out}} \right| \left(\frac{\beta_{in}}{\beta_{out}} \right) \left(Y_{p,\beta_{in}=-\beta_{out}} - Y_{p,\beta_{in}=0^\circ} \right) \right] \left(\frac{5 t_{max}}{c} \right)^{-K_m \frac{\beta_{in}}{\beta_{out}}}, \\ &= (s/c, t_{max}/c, \beta_{in}, \beta_{out}, \psi_Z). \end{aligned} \tag{21}$$

Carrying on with the auxiliary factor arrangement of Equation (3), several minor changes were performed.

1. Metal angle θ_{in} in Equation (21) was replaced by a design flow angle β_{in}. Practically, a better continuity in design workflow is gained by focusing on the flow angles first and deriving the metal angles afterward. Modern turbines tend to integrate little negative incidence to enable low loss in off designs. Proceeding with θ_{in} would, rather, require extra iterations in the preliminary design process.
2. $Y_{p,\beta_{in}=0^\circ}$ and $Y_{p,\beta_{in}=-\beta_{out}}$ in Equation (21) were scaled by a common s/c. Before developing the modifications, the context in which they were built is reviewed and compared to current practice. During the 1940s, blade profiling was an empirical science. It consisted of a selection from a family of standardized profiles and was arranged into cascade configuration with little allowable change. This approach was inherited from axial compressors and guaranteed cost-effectiveness as it facilitated manufacture. It was impossible to grasp the trend of cascade performance without resorting to cumbersome trial and error wind tunnel tests until the determination of a competent profile. This substantially contrasts with modern profiling techniques, which offer close monitoring and automated optimization of the blade surface velocity distribution. $Y_{p,\beta_{in}=0^\circ}$ and $Y_{p,\beta_{in}=-\beta_{out}}$ were certainly obtained from competent but obsolete profiles, in which blade surface velocity distributions or efficiencies have become unacceptable according to modern state of the art standards [34]. As they form the cornerstone of Equation (2), it would be unreasonable to initiate large modification at the risk of disrupting the auxiliary factor arrangement in Equations (3) and (20). Instead, a scaling technique with a reference s/c, which is analogous to that applied to compressor performance maps, is proposed. In a design process, s/c is set following a trade off between efficiency and cost. If efficiency consideration prevails, the optimum s/c that minimizes profile loss, in this case of Equation (2), is chosen, so that any s/c departure results in profile loss increase or simply efficiency deterioration. However,

the optimum s/c of $Y_{p,\beta_{in}=0^\circ}$ and $Y_{p,\beta_{in}=-\beta_{out}}$ are fixed and specific to competent profiles. The issue would then be its insensitivity to other types of profile. With this in mind, a reasonable approach that maintains the $Y_{p,\beta_{in}=0^\circ}$ and $Y_{p,\beta_{in}=-\beta_{out}}$ trend and scales the optimum pitch to chord ratio s/c_{AM} of Equation (2) to a new optimum s/c is proposed. The purpose is to extend Equation (21) to other profiles in which optimum s/c abides by different design rules. Among these, the prominent Zweifel criterion [11] is chosen to inherit its flexibility and its incompressible is generalized to:

$$s/c_Z = \frac{1}{2}\frac{b}{c}\frac{\psi_Z}{|\frac{1}{\mathrm{AVR}}\tan\beta_{in} - \tan\beta_{out}|\cos^2\beta_{out}}, \tag{22}$$

introducing the axial velocity ratio AVR as an additional design parameter. An ψ_Z beyond the range of [0.6–0.8] recommended by Zweifel is chosen, to achieve the higher optimum pitch to chord ratio s/c_Z in modern turbines. The vital scaling factor is:

$$\begin{aligned} f_{s/c} &= \frac{s/c_Z}{s/c_{AM}}, \\ &= f(s/c, \beta_{in}, \beta_{out}, \mathrm{AVR}, \psi_Z, \gamma), \end{aligned} \tag{23}$$

which is multiplied to the s/c_{AM} of Equation (21). Note that $Y_{p,\beta_{in}=0^\circ}$ and $Y_{p,\beta_{in}=-\beta_{out}}$ are fitted as polynomials about their respective optimum s/c (the fitting formulae of Tournier and El-Genk [45], Korpela [46], Aungier [6] and Concepts/ETI [47] were tested at extreme $\beta_{out} = 30^\circ$ and $\beta_{out} = 80^\circ$; the Tournier and El-Genk performed best), so that the scaling process does not alter their slope. As demonstrated, the original and scaled $Y_{p,\beta_{in}=0^\circ}$ and $Y_{p,\beta_{in}=-\beta_{out}}$ are depicted at exit flow angles $\beta_{out} = 50^\circ$ and 70° in Figure 2, with the $\psi_Z = 1$ typical of modern turbines.

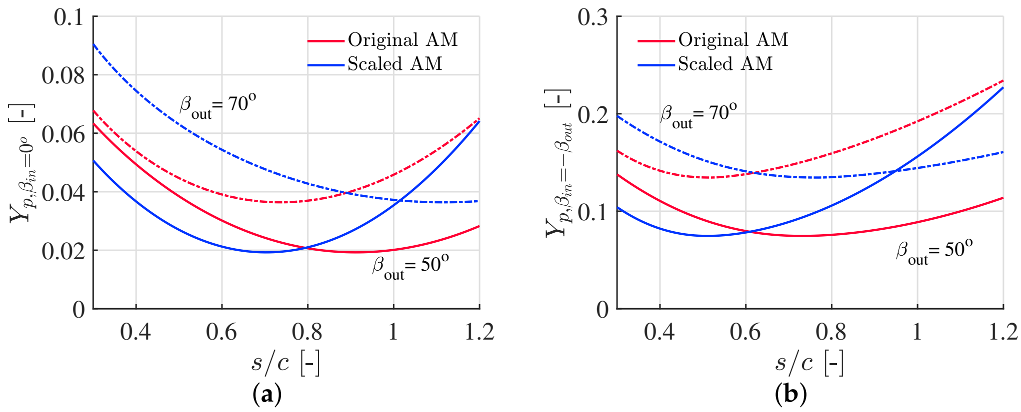

Figure 2. Optimal pitch to- hord ratio matching of AM profile losses [2] with $\psi_Z = 1$. (**a**) Nozzle $\beta_{in} = 0^\circ$. (**b**) Impulse $\beta_{in} = -\beta_{out}$.

Both Figure 2a,b are consistent on the minimum shift. At $\beta_{out} = 70^\circ$, a larger s/c can be achieved with better boundary layer flow control during blade profiling. However, at $\beta_{out} = 50^\circ$, a lower s/c is resorted tp, in order to satisfy $\psi_Z = 1$. This is an undesirable solution, as this would add structural weight. A cost-effective constraint is imposed to refrain $f_{s/c} \geq 1.1$.

3. The Reynolds correction factor K_{Re} was adjusted to suction surface length and becomes a function of the suction surface Reynolds number Re_s. Suction surface momentum thickness could be responsible of up to 90% of the profile loss [32], the suction surface flow should logically be prioritized.

4. Incidence loss Y_{inc} replaces the incidence factor K_i of Equation (3) and acts as a fully independent, contributing to the profile loss. According to Moustapha et al. [15], modern turbines are designed with relatively thicker leading edges and smoother front curvatures, to retard boundary layer separation over a wide range of incidence angles and to keep loss at low level. This feature can not be reflected in the conservative K_i. In this regard, Benner et al. [48] formulated a polynomial incidence loss Y_{inc} compatible with KO and used in Equation (20).
5. The trailing edge loss $Y_{te,Ag}$ of Equation (7) is insensitive to change of turbine operating conditions and, thus, was deemed inappropriate for modifications. As an alternative, the Y_{te} of KO, which encompasses many key aerodynamic parameters, is considered:

$$\Delta\Phi_{te,KO} = \Delta\Phi_{te,\beta_{in}=0^\circ} - \left|\frac{\beta_{in}}{\beta_{out}}\right|\left(\frac{\beta_{in}}{\beta_{out}}\right)\left(\Delta\Phi_{te,\beta_{in}=-\beta_{out}} - \Delta\Phi_{te,\beta_{in}=0^\circ}\right). \tag{24}$$

The replacement of θ_{in} by β_{in} follows the same reasoning behind Equation (21). Drawing on the profile loss of AM in Equation (2), KO blended the exit boundary layer mixing and base pressure losses of nozzle and impulse blades [5]. Instead of a subtraction, as in Equation (3), virtual correction of Y_p to $t_{te}/s = 0$ produces a multiplication by 0.914 in Equation (20). The latter corresponds to the value of K_{te} proposed by AM in Equation (5) at standard $t_{te}/s = 0$ [2]. Now, the conversion of Equation (24) to Y_{te} involves $M_{r,out}$ [49]. This is a property specific to the total pressure loss coefficient and cannot be counted as part of the correlation. However, recent literature has proven its reliance on $M_{r,out}$ but has not delivered any correlation compatible to the AM family [50]. Conveniently, Equation (24) was acquired on low speed tests in the same way as Equation (2). This implies that auxiliary factors defined for the profile loss can be reasonably extended to the trailing edge loss. Considering the relevance of compressibility and Reynolds effects, Equation (24) is revamped into

$$\begin{aligned} Y_{te,Enh} &= K_M K_p K_{Re} Y_{te,KO}, \\ &= f(\beta_{in}, \beta_{out}, t_{te}/o, M_{r,in}, M_{r,out}, Re_s, e/c). \end{aligned} \tag{25}$$

4. Revised Secondary Loss

In light of the issues disclosed earlier in Equation (9), its terms are overhauled. The purpose is to determine a better product of loading and displacement supported by a robust physical basis and depart from the approach used in Equation (16). The latter implies that each contribution has to fully be independent, as in Equation (1). Interestingly, there was a formulation anterior to Equation (8) found in early works [24,33]:

$$Y_{s,AM} = 0.04\left(1 - \frac{\theta_{in}}{\beta_{out}}\right)C_{L,out}^2, \tag{26}$$

using the lift coefficient based on the outlet velocity

$$C_{L,out} = 2\frac{s}{c}(\tan\beta_{in} - \tan\beta_{out})\frac{\cos^2\beta_{out}}{\cos\beta_m}. \tag{27}$$

Unfortunately, Equation (26) was abandoned in favor of the model of Carter [35] because it owns a firmer theoretical background and provides common ground for future compressor and turbine models, according to AM [34]. Contrary to their expectation, axial compressors and turbines have not taken the same course of evolution. As odd as it may be, there is a soundness in Equation (26) in the present context. In particular, $C_{L,out}$ is consistent with turbine analysis, which is not the case with Z of Equation (8), which relies on $C_{L,m}$ in Equation (10).

The secondary loss improvement begins with $C_{L,out}$ rearranged and generalized into the lift solidity coefficient

$$\frac{C_{L,out}}{s/c} = \left(1 + \frac{1}{\mathrm{AVR}}\right)\left(\frac{\kappa}{\mathrm{AVR}} \tan\beta_{in} - \tan\beta_{out}\right)\frac{\cos^2\beta_{out}}{\cos\beta_m}. \tag{28}$$

Assuming AVR $= \kappa = 1$, Equation (27) is recovered. Modern turbines possess a meridional flowpath that forces the radial shift of streamlines such that $\kappa \neq 1$. The latter triggers the Coriolis force and may lower work output [51]. Moreover, expansion through each row inevitably accelerates the flow and, thus, invariance of AVR even in early design stages, which thus constitutes a poor assumption. This aspect would serve in the subsequent evaluation of the correlation reliability. In addition, β_m is also generalized to:

$$\beta_m = \tan^{-1}\left(\frac{\frac{1}{\mathrm{AVR}}\tan\beta_{in} + \tan\beta_{out}}{1 + \frac{1}{\mathrm{AVR}}}\right). \tag{29}$$

Elaborated models of the endwall vortices have been produced since then, to substitute the classical secondary flow theory. Among these, the passage vortex penetration depth of Sharma and Butler [12], later enhanced by Benner et al. [13], is proposed as the replacement to λ_{AM}:

$$\begin{aligned}\frac{Z_{te}}{H} &= \frac{0.1F_\theta^{0.79}}{\sqrt{\mathrm{CR}}(H/c)^{0.55}} + 32.7\left(\frac{\delta^*}{H}\right)^2, \\ &= f(H/c, \delta^*/H, \beta_{in}, \beta_{out}, \gamma, s/c, \mathrm{AVR}).\end{aligned} \tag{30}$$

Once the incident endwall flow impinges on the blade, a first separation occurs at the leading edge, creating a horseshoe vortex, as illustrated in Figure 3a. Under passage pressure gradient and crossflow friction, the pressure leg is progressively strengthened and pushed towards the adjacent blade suction side. Meanwhile, the suction leg remains near the suction side wall. Eventually, both legs of opposite vorticity coincide at the minimum pressure point. The suction leg starts to orbit around the dominant pressure leg, also identified as the passage vortex. The latter draws a demarcation line S4 on the blade suction side. Sharma and Butler assumed symmetric and linear S4, beginning at the leading edge and forming a triangle, as shown in Figure 3b. Z_{te}/H corresponds to the width of the passage vortex taken at the trailing edge. It also differs from λ_{AM} by the weight attributed to the parameters. For instance, AM prioritized the area ratio A_{out}/A_{in} over blade turning $\beta_{in} + \beta_{out}$, as there was only weak evidence on the influence of blade loading [34]. On the opposite, the genetic algorithm used by Benner et al. identified a stronger influence of the blade tangential force F_θ, rather than the convergence ratio CR, analogous to A_{out}/A_{in}.

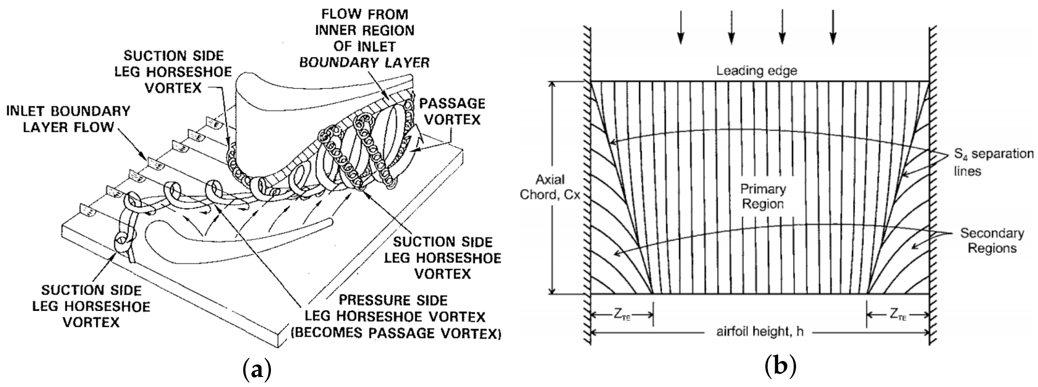

Figure 3. Endwall vortices model. (**a**) New secondary loss model [12]. (**b**) Passage vortex penetration depth [13].

Coull and Hodson [10] pointed out the absence of directives in the calculation of the upstream displacement thickness δ^*/H. This is a minor issue, as classical formulae or reasonable estimates could be resorted to. However, it is still unable to consider downstream endwall loss increase [18]. In a turbine environment, this issue becomes less relevant, as vortex flow is disrupted by succeeding blade rows distanced by a short row gap. The threshold of Equation (30) is $Z_{te}/H = 0.5$, above which the merging of the endwall vortices takes place and produces distinct flow dynamics.

An additional consideration is made on the aspect ratio H/c. Enlarging blade height H and shortening blade chord c both increase H/c but affect secondary loss in different ways [34]. This problem was raised in the early cascade tests of Kraft [52], which exposed the insensitivity of the secondary loss under the change of c. The traditional interpretation reflected by the auxiliary factor K_{AR} in Equations (17) and (19) is that secondary loss is inversely proportional to H/c. This is valid when H is varied but no special regard to c has been made. However, as H/c approaches 0, K_{AR} tends to infinity and vice versa. This contradicts the real physics of the secondary flow. Teia even showed that the structure of the endwall vortices is unaltered by the change of H beyond a certain critical aspect ratio in his Figures 10–12, page 25–26 [42]. He deduced that interaction between the endwall vortices is absent and, thus, secondary loss should remain constant. Below a certain critical aspect ratio varying H, the vortices merge together and amplify loss. His observation offers new insights into the highlighted inconsistency but lacks key verification. Notably, correlation between vortices' interaction and loss was not established and this can hardly argue secondary loss insensitivity for all H/c before merging. In addition, no means were provided to estimate his critical aspect ratio. Drawing partially on his observation, invariance to H/c above $H/c = 2$ in Equation (30) is imposed. $H/c = 2$ corresponds to the traditional threshold below which the slope of K_{AR} becomes sharper. Concurrently, the database size bias of Equation (30) reduces its certainty beyond the same threshold [13]. At this stage, it is cautiously advanced that loss amplification occurs even before the merging of the vortices within $H/c \leq 2$. The problem with c remains unsolved.

Replacing Equation (8), the basic secondary loss is

$$\begin{aligned} Y_{s,b} &= \frac{1}{2}\frac{Z_{te}}{H}\left(\frac{C_{L,out}}{s/c}\right)^2, \\ &= f(H/c, \delta^*/H, \beta_{in}, \beta_{out}, \gamma, s/c, \mathrm{AVR}, \kappa), \end{aligned} \tag{31}$$

accounting for the pair of endwall vortices and their core located at $Z_{te}/2H$ as in Figure 3b. This respects the structure of lost work with loading and displacement parameters. The square of $C_{L,out}/(s/c)$, as in Equation (26), is inherited from the classical lifting-line theory, which associates the endwall and induced vortices. It yields values which are lower than Z by several order of magnitude, hence predominance of $C_{L,out}/(s/c)$ over other parameters is naturally prevented

The independence to s/c in Equation (19) has been criticized, as this does not fit reality [41,53]. Practice refers to the optimum s/c with profile loss consideration only, there are still no available studies, to this day, that have addressed an overall optimum for both profile and secondary losses [19]. The tangential force F_θ of Equation (30) utilizes s/c as loading indicator and is unable to serve this purpose. As a reasonable attempt to incorporate the intensification of secondary loss caused by deviation from the profile optimum s/c, an auxiliary factor is proposed

$$\begin{aligned} K_{sc} &= 1 + 10\left(1 - \frac{s/c}{s/c_Z}\right)^2, \\ &= f(s/c, \beta_{in}, \beta_{out}, \mathrm{AVR}, \psi_Z, \gamma). \end{aligned} \tag{32}$$

This polynomial expression was acquired by fitting the cascade data of Perdichizzi and Dossena [41], as shown in Figure 4.

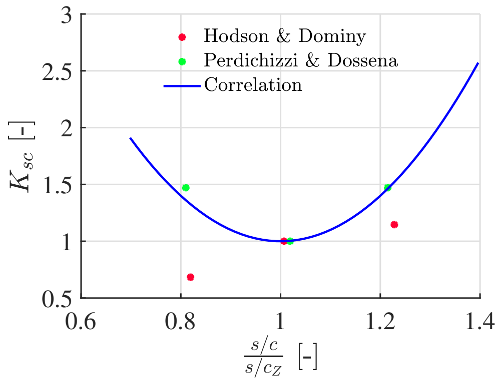

Figure 4. Optimum pitch to chord ratio auxiliary factor for secondary loss.

Tests were conducted for $s/c = 0.58, 0.73, 0.87$ and $i \in [-60\text{–}+35]^\circ$. The highlighted points result from averaging over the incidence range and normalizing by s/c_Z with $\psi_Z = 0.6$ such that a clear parabola could be drawn. The data of Hodson and Dominy [53] were also exposed and normalized with $\psi_Z = 0.9$, for comparison. According to the trend, it is seen that their LPT profiles were not optimized at nominal s/c and, thus, their results are omitted. The magnitude of Equation (32) is restrained to 1.5 beyond the range [0.8–1.2] as a precaution, given the scarcity of data. Lastly, the enhanced secondary loss, keeping the same arrangement as Equation (19), is updated as

$$\begin{aligned} Y_{s,Enh} &= K_{sc} K_p K_{Re} \left(\frac{Y_{s,b}^2}{1 + 7.5 Y_{s,b}^2} \right)^{\frac{1}{2}}, \\ &= f(s/c, \psi_Z, \gamma, M_{r,in}, M_{r,out}, Re_s, e/c, H/c, \delta^*/H, \beta_{in}, \beta_{out}, \mathrm{AVR}, \kappa). \end{aligned} \tag{33}$$

Further discussions regarding recent works are carried on. Teia [42] stipulated that profile loss should increase with H/c. He argued that increasing H incurs additional loss, as the boundary layer covers more surface area. This implies a 3D effect which violates the 2D spanwise uniformity of the profile loss assumed in Equation (1). A similar attempt was done by Benner et al. [54], with their alternative loss breakdown

$$Y_t = Y_p \left(1 - \frac{Z_{te}}{H} \right) + Y_s. \tag{34}$$

The boundary layer flow was treated separately in accordance to the area division on the suction side in Figure 3b. They stated that their secondary loss correlation includes the profile loss of the secondary regions, which is unlikely since their genetic algorithm search removed the blade skin friction during the development of their correlation. In that sense, the net profile loss is confined within the primary region delimited by S4. Although intuitive, these results are not compatible with older correlations, especially when the Y_p of Equation (34) is still that of KO.

To ascertain the credibility of the update, it has to achieve statistical significance and thus requires a large database. A major challenge in this framework is to gather a sufficient number of public turbine test cases to possibly enable unbiased analysis. A previous study [23] collected 33 subsonic cascades (15 static and 18 rotating) partitioned from single stage turbines. The same approach is adopted and the previous cascade database is enlarged to 109 specimens (54 static and 55 rotating) to enhance representativeness. Their key design parameter range is summarized in Table 1.

Table 1. Design parameter range of the cascade database.

Parameters	Min	Max
s/c	0.498	0.974
H/c	0.456	6.493
$M_{r,in}$	0.071	0.649
$M_{r,out}$	0.149	1.280
$\beta_{in} + \beta_{out}$	45.6°	138.9°
Re	4.538×10^4	6.025×10^6
Re_s	5.487×10^4	1.1185×10^7

Although it was advanced that reliability should be prioritized over the accuracy in the early review, both aspects would be investigated. For this purpose, high fidelity CFD simulations were conducted on the cascades and the solutions would serve as a benchmark in the analysis.

Although the clearance leakage loss Y_{cl} is not addressed in this paper, it is fundamental to select a compatible leakage loss model to complete the system of Equation (1). For this purpose, the recent correlations of Yaras and Sjolander [55] or Farokhi [56] are recommended.

5. Numerical Method

Since numerical steady solutions serve in determining Y_t, their credibility has to be guaranteed. At issue is their overriding dependence upon numerical discretization and turbulence modelling [57]. Without proper verification and validation, any produced solutions would be untrustworthy [58]. In this regard, a previous study [23] adopted the systematic V and V procedure [59] to identify the numerical scheme (mesh and turbulence model) best suited for the simulation of turbine aerodynamics. It was performed on the Aachen turbine rotor test case [60] with NUMECA FINE/Turbo [61] and presented an on design numerical error of 3.79% the experimental value. The latter is considerably lower than the accuracy standard of ±15% of the correlations [34,38], therefore justifying the use of CFD in the assessment.

The computations were run with the commercial package NUMECA FINE/Turbo [61] whose code architecture is capable of maximum second order accuracy. In order to capture anisotropy, and impact of curvature and body forces on turbulence, the proprietary separation sensitive corrected explicit algebraic Reynolds stress model (SSC-EARSM) was chosen. Compared to the conventional EARSM model [62], this was calibrated by scale adaptive simulation to increase turbulent mixing in the flow separation region and enhance the near wall behavior of anisotropy. Single blade passage meshes were generated with the semi-automatic mesher AutoGrid5. O4H topology, which comprises batches of curvilinear structured hexahedral blocks, was adopted. A large portion of cells were clustered at the wall boundaries and plane intersections to enable, first, inner cell spacing characterized by $y^+ \approx 0.8$ within the viscous sublayer. The employed mesh resolution was about 2.7×10^6 nodes. To ensure algorithm robustness, a uniform profile of absolute total temperature and pressure was imposed at the inlet patch, placed at one chord upstream of the leading edge. This also guarantees the control of the endwall boundary layer over the distance separating the inlet patch to the blade leading edge and enables the use of classical formula in the δ^* estimation in Equation (30). Static pressure was subsequently prescribed at the outlet patch placed at one chord downstream of the trailing edge. This distance should enable mixed out solutions at the outlet. Periodic boundary conditions were imposed on the circumferential patches of the control volume. All simulations were performed with real gas in on design conditions, unless specified otherwise.

6. Correlation Accuracy

Although it has been advanced that correlation accuracy should not be prioritized, the extreme case with 100% error is not tolerable either. In that sense, the limit at which inaccuracy fails the correlation has to be evaluated. For this purpose, the previous gauge with the probability ΔP_{tol} of reaching a tolerance interval of ±15% error is reused [23], this is depicted in Figure 5. This conforms to the aforementioned accuracy standard of ±15% [38] and accommodates numerical error uncertainties.

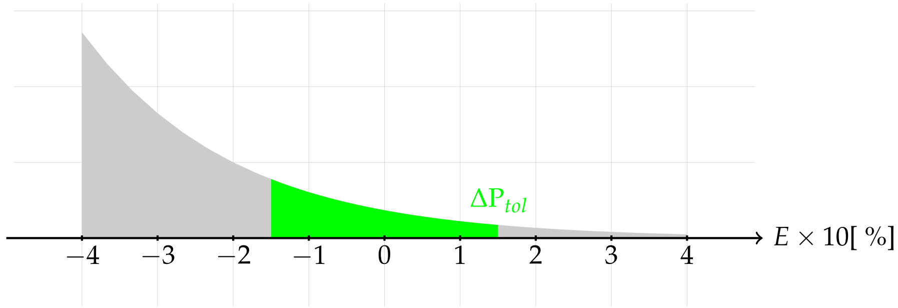

Figure 5. Tolerance interval for correlation accuracy evaluation.

The assessment relies on straightforward descriptive statistics. The latter require a bounded quantity following a near normal distribution and including Equation (1). Thus, the relative error normalized by the benchmark CFD solutions is

$$E = \frac{Y_{t,num} - Y_t}{Y_{t,num}}. \tag{35}$$

with the large database available, a z-distribution is assumed [63].

The update is assessed together with its original form in Figure 6. By comparing the predicted loss of each cascade, the depicted trend in Figure 6a indicates a higher estimation by the enhanced correlation. Distinct disparities occur at high loss levels, whereas most points are clustered below the bisection at low levels, within a ±0.05 band. Hence, Ag and its update moderately agree for low loss only. As per the convention for scatter plots, the centered bar represents the mean and the other smaller and larger bars delimit the 99% confidence interval and standard deviation, respectively. Figure 6b uncovers a significant difference between Ag and its update, with approximately 10% distance separating their confidence interval. Both populations have comparable spreads but that of Ag is largely decentered, unveiling a systematic underestimation from the Ag correlation. Their difference produces a coherent shift of its mean to the negative side. However, contrary to any expectation, its spread has not shrunk, implying that the update has inherently departed from its original model in terms of turbine aerodynamics interpretation. A priori, if accuracy has to be improved, then the correlation should have its relative error centered on 0 and standard deviation within ±15%, to deliver at least $\Delta P_{tol} = 66\%$. The numerical values are gathered in Table 2 and include the ΔP_{tol} of each distribution.

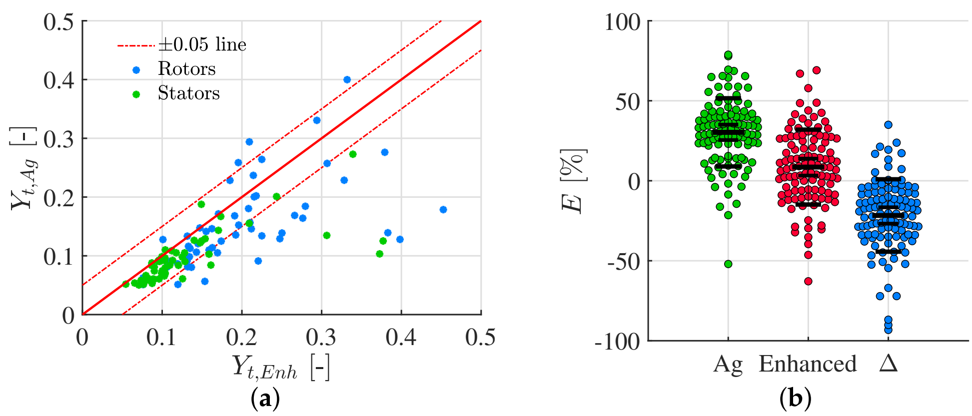

Figure 6. Comparison of Ag and enhanced correlations. (**a**) Total loss. (**b**) Total loss relative error.

Table 2. Statistical solutions of the axial cascade database.

Method	Descriptive Statistics		
Parameters	$\bar{E}$ [%]	σ [%]	ΔP_{tol} [%]
Ag	30.255	21.308	22.018
Enhanced	8.548	23.409	45.136
Δ	−21.707	22.634	33.107

With the Ag correlation, it is possible to achieve the required accuracy with approximately 25% chance. This result is opposite to the previous analysis, which reported an optimistic $\Delta P_{tol} = 45.13\%$ while retaining a comparable $\sigma = 23.41$ over 33 cascades [23]. It is very likely that the mean is susceptible to sample size bias, while the spread remains invariant. The enhanced correlation outperforms by doubling ΔP_{tol} with a better position of its mean error. This result has to be handled with care, as this would change with another comparable cascade database with a shift of the mean error. On the other hand, the spread manifests as a barrier marking the limit of low fidelity models. For this reason, accuracy should be relegated to higher order methods.

7. Correlation Reliability

Adopting the approach of Horlock [64] and Coull and Hodson [32], trend consistency is evaluated with the flow coefficient ϕ and stage loading ψ. The latter condition the turbine stage velocity triangle and efficiency. Their early selection is guided by the famous Smith chart [14], after fixing the stage number.

As a reminder, Figure 7 was established by tests on 70 cold single stage turbines which reactions varied from 20% to 60%. These were designed with AVR = 1 and zero incidence. Coull and Hodson supplemented the blade profiles associated to different areas of the chart. The top left area is characterized by the highest turning and lowest efficiency airfoils to satisfy the loading requirement. In this regard, accrued interblade passage convergence is required to guide reduced momentum flows. Nevertheless, flow turning can be alleviated for the same loading and efficiency by increasing ϕ and thus transiting to the top right area. Eventually, the bottom area is characterized by low turning and higher efficiency airfoils and the same consideration concerning the flow passage configuration.

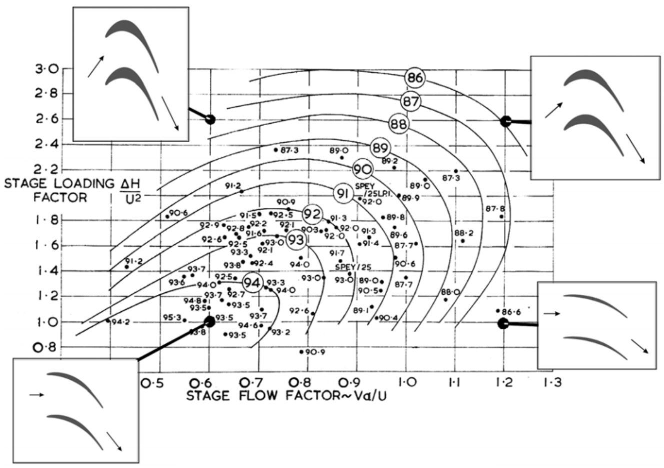

Figure 7. Smith chart calibrated to zero tip loss and 50% reaction [14,32].

To demonstrate reliability, the enhanced correlation is expected to reproduce the same topology by varying ϕ and ψ, as attempted by CC [17] and KO [5]. For this purpose, the analysis begins with the design of a single LPT stage using the setting of Coull and Hodson to acquire a common basis for comparison and explore the LPT for which the AM correlations are known to fail [10]. Repeating stage, 50% reaction, a constant hub to tip ratio of 0.75 and parabolic camber are assumed. The first stage power requirement and inlet boundary conditions are taken from the GE E3 LPT [65]. The design parameters s/c, β_{out}, velocity ratio VR$= W_{out}/W_{in}$ and H/c of the LPT rotor are plotted in Figure 8 over the same ψ and ϕ range as the Smith chart, for reference. Consecutively, the LPT isentropic efficiency is derived.

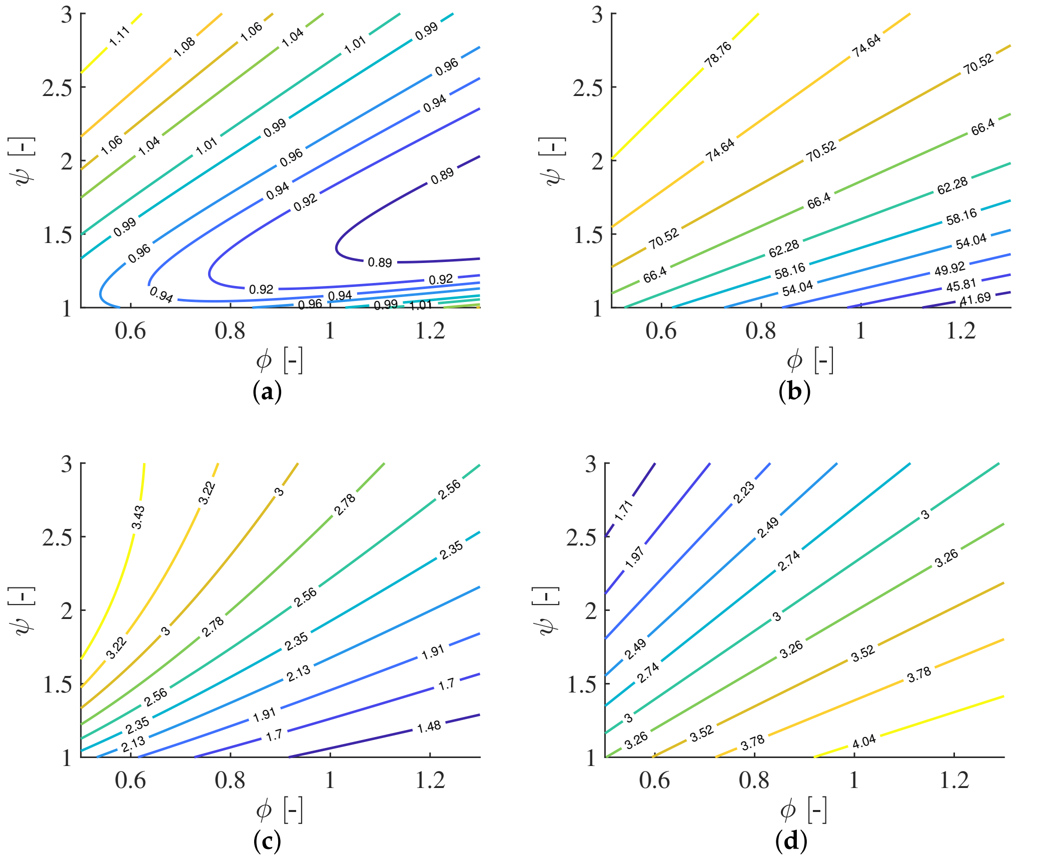

Figure 8. Velocity triangle and geometric parameter ranges of the LPT rotor. (**a**) Pitch to chord ratio s/c. (**b**) Exit flow angle β_{out}. (**c**) Velocity ratio VR. (**d**) Aspect ratio H/c.

First, considering the profile loss efficiency in Figure 9, both contour plots unsurprisingly share the same topology. Equations (2) and (21) differ by minor calibrations involving the Zweifel criterion [11] and extending the auxiliary factors to Equation (24). Furthermore, their bottom right area is identical, since Zweifel criterion matching is disabled for low turning profiles at $f_{s/c} > 1.1$. The abrupt break of the contour 0.02 arises from K_{mod}, which alters its value when departing from nozzle profiles at low ψ [37]. In Figure 9a, profile loss is minimized for most of the bottom area, reflecting low turning profiles, as shown in Figure 8b. Greater ψ and fewer losses are feasible by increasing ϕ but at expense of lower s/c, as in Figure 8a. Loss is aggravated towards the top left area, which conforms to Figure 7. Figure 9b stands out with its comparatively lighter gradient, induced by the adequate application of $f_{s/c}$. With the exception of the bottom right area and according to the results of Coull and Hodson [32], a loss level comparable to that of the semi-analytical correlations of Denton [31] and Coull and Hodson [10], in Figure 10a,b, page 7, respectively, is achieved.

Then, secondary losses differ in all possible aspects in Figure 10. The Ag secondary loss [6] remains low for most of the domain and increases towards the top left area in Figure 10a. This pattern is not shared by other AM family correlations [10]. Further insights are offered by analyzing the components of Equation (8). Here, λ_{AM} displays a topology similar to that of Figure 7 in Figure 11a. Its minimum is reached at the bottom left area and, curiously, remains invariant towards the top right direction. Meanwhile, amplification takes place in all other directions, switching from curved to straight contours. On the other hand, Z progressively grows accordingly, along ψ, to reach the steepest straight contour in the top left area in Figure 11c. With a difference of $O(10^3)$, it naturally plays a predominant role in the product of Equation (8) and dictates the resulting topology. Thus, Figure 10a disregards most features of Figure 11a and highlights losses with contours that are curved by the auxiliary factors and the square root of Equation (19). Conversely, the lowest loss is produced at greater ψ and gradually intensifies towards the bottom right area in Figure 10b.

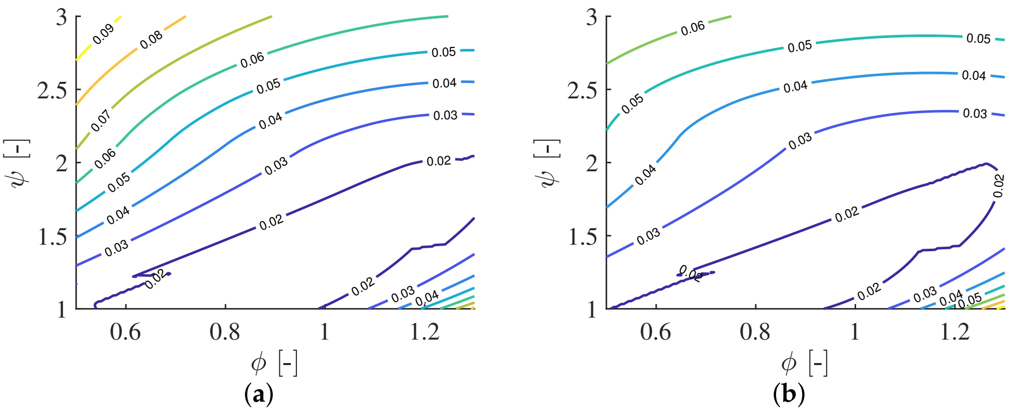

Figure 9. Profile loss efficiency with $\psi_Z = 1.1$, AVR = 1, $i = 0$, $H/b = 6.5$, 4.6 for stator and rotor. (**a**) Aungier [6]. (**b**) Enhanced.

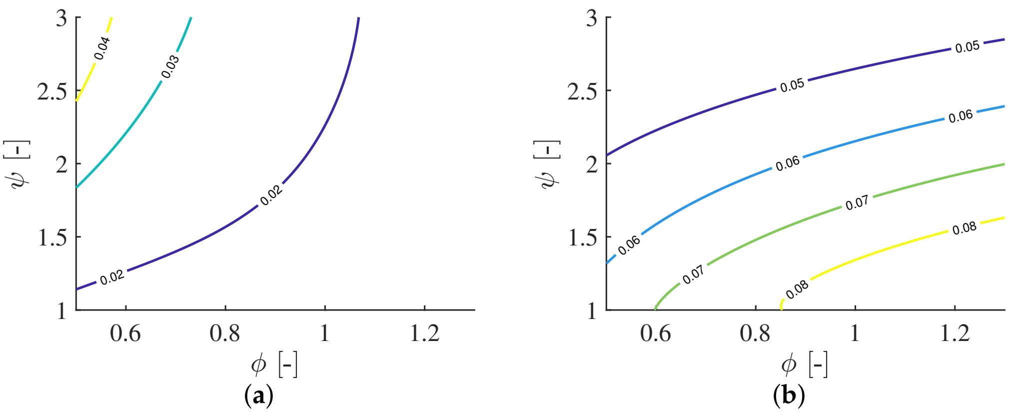

Figure 10. Secondary loss efficiency with $\psi_Z = 1.1$, AVR = 1, $H/b = 6.5$, 4.6 for stator and rotor. (**a**) Aungier [6]. (**b**) Enhanced.

The central question to be posed now is which correlation conforms to reality? Back to Figure 11a, λ_{AM} is supposed to reflect the endwall vortices. In this regard, the increase in the top left area is consistent, since it is backed by a sharper exit angle in Figure 8b and lesser aspect ratio in Figure 8d. However, the other increase in the bottom right area is unlikely. It is impossible to magnify the endwall vortices by decreasing turning/loading, increasing aspect ratio and also lowering VR in Figure 8c. Moreover, a higher ϕ should not favor the growth of secondary flows in the flow passage, as these are downwashed through considerable momentum convection [7]. With these points in mind, it is seen that the monotonous penetration depth of Figure 11b better matches the topology of Figure 8b–d. The contour slope disruption in the top left area is triggered by the aspect ratio variation for $H/c < 2$, ensuring discussion over the results of Teia [42]. Once again, there is a clear divergence between the blade loadings in Figure 11c,d. Contrasting with Figure 11c, the maximum is located in the bottom right area. This feature comes from the s/c at the denominator in Equation (28) and is substantiated by Figure 8a, in which the minimum occupies the same area. Z originally accounted for s/c as uncovered in Equation (13) but dispensed with its contribution, as confirmed herein. Furthermore, secondary loss increase under high ϕ and low ψ was also produced by the trusted CC [17] and Traupel [25] correlations [10]. Despite the absence of similarity with Figure 7, consistency in the enhanced correlation is comparatively augmented. In particular, the difference between the components of Equation (19) is mitigated to $O(10)$.

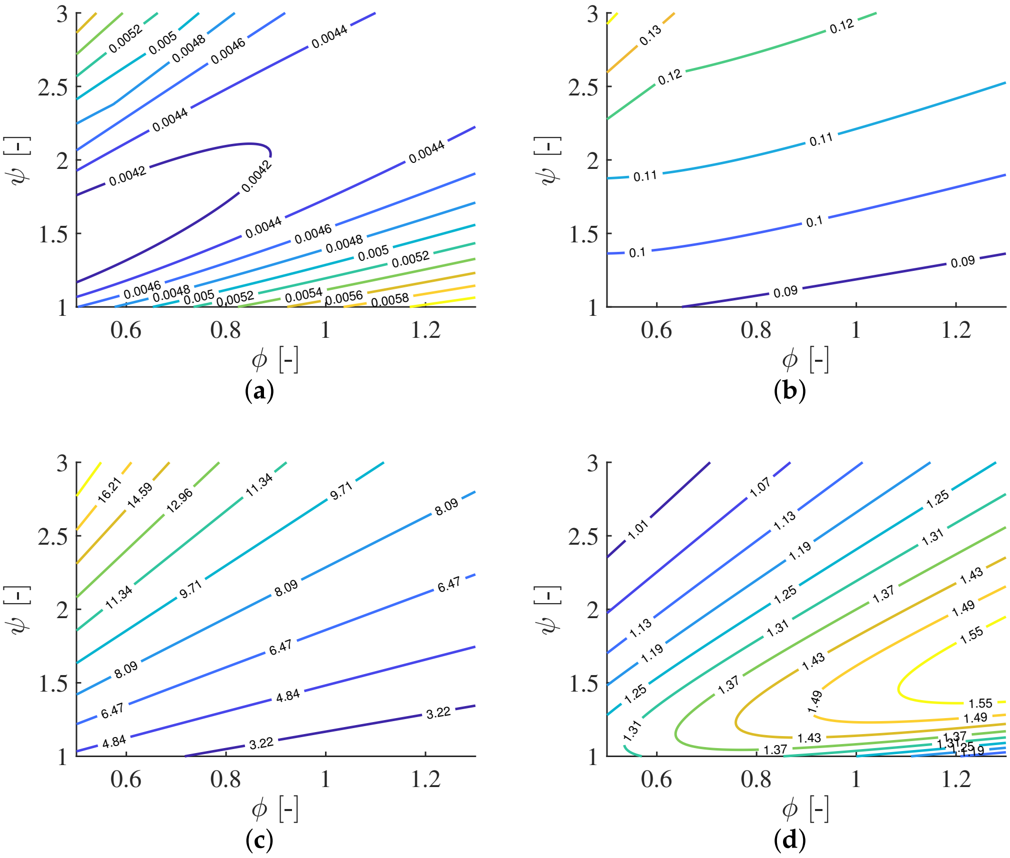

Figure 11. Rotor secondary loss components with $\psi_Z = 1.1$, AVR $= 1$, $H/b = 4.6$. (**a**) Ainley parameter λ_{AM}. (**b**) Vortex penetration depth $Z_{te}/2H$. (**c**) Ainley loading Z. (**d**) Generalized lift solidity coefficient $C_L/s/c$.

Eventually, the isentropic efficiency key to correlation reliability is depicted in Figure 12. The trend of Ag in Figure 12a is clearly driven by the profile loss in Figure 9a. In that respect, the bowed contours that are supposed to be inscribed in the domain of Figure 7 are stretched towards higher ϕ. As a consequence, losses induced by large ϕ are underestimated by the correlation. In addition, the update reveals to be more conservative in the quantification of the losses, as the first identified contour is 0.91 in Figure 12b. The latter exhibits an almost complete bow but is not comparable to those of the Smith chart, as it covers too much area. Hence, it can only enable a global trend consistency. Although overstretching to high ϕ is reduced, its expansion occasions over and under estimations in the bottom and top areas, respectively. Variation of contour level or sensitivity to design parameters is lessened. These weaknesses are occasioned by the secondary loss in which $H/c = 2$ is held constant for most of the domain, as shown in Figure 11b. This is somewhat expected, as Equation (30) of Benner et al. [13] was not intended for the current treatment regarding H/c. The model's conservativeness could be alleviated through a larger H/c, if justified. For now, the threshold $H/c = 2$ is untouched, as the reasonable conservativeness in preliminary design provides an adequate margin for subsequent modifications.

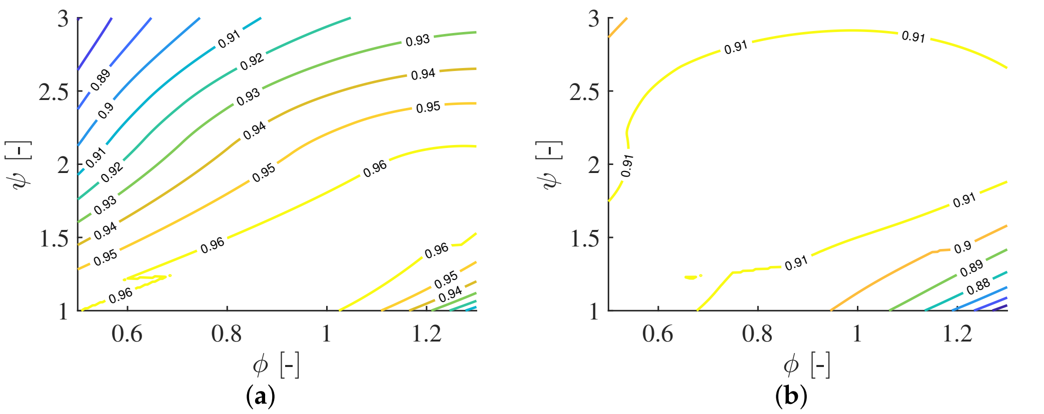

Figure 12. Isentropic efficiency with $\psi_Z = 1.1$, AVR $= 1$, $H/b = 6.5$, 4.6 for stator and rotor. (**a**) Aungier [6]. (**b**) Enhanced.

The enhanced correlation has introduced additional design parameters or degrees of freedom, in hopes of reaching a better control on design. These are summarized in Appendix A Table A1 and their number amounts to three to five for the profile and secondary losses, respectively. The following analysis retains four static and rotating cascades [26,60,65,66] with distinct κ and with their operating conditions altered with a back pressure within $\pm 10\%$ of its nominal value. This aims to evaluate the change of Y_t over the prescribed operation range, drawing on the approach of Wei [9]. Again, CFD solutions form the benchmark. AVR determined in the early velocity triangle and knowingly set to unity in the AM correlations is concurrently highlighted to demonstrate its relevance as a design parameter. The results of the static and rotating cascades normalized by on design CFD values are depicted in Figure 13. The cascades are not identified to their references in the plots to foster randomness, as reliability must not be biased by the turbine origin.

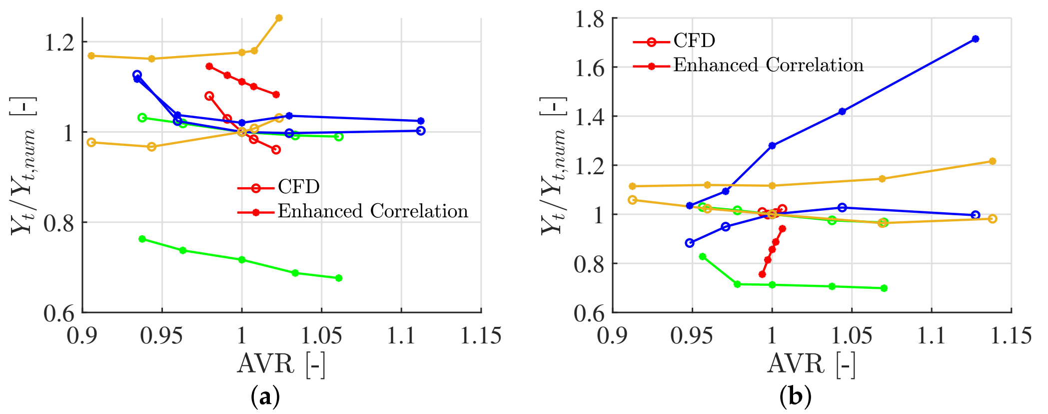

Figure 13. Total loss variation of four cascades. (**a**) Stators. (**b**) Rotors.

The distance separating each pair of curves relates to accuracy. It is worth mentioning that two out of four cascades achieve the early tolerance interval and this conform with the estimated $\Delta P_{tol} = 45\%$. AVR varies for different operating conditions and extends as far as 15% its nominal value in Figure 13b. This parameter has demonstrated its nontriviality and hence justifies the generalization of Equations (22) and (28). By diminishing the back pressure, AVR increases and vice-versa. For the static cascades in Figure 13a, the trend of each pair of curves similarly results in an acceptable global consistency. If strict consistency is imposed, then the curves should have synchronous slopes that conserve their separation at each variation. Whereas, for the rotating cascades in Figure 13b, serious trend disruptions are displayed introducing undesirable uncertainties. One cascade undergoes slope switchover to negative values at AVR $= 1.05$. Moreover, there are two cascades for which a considerable slope mismatch is seen. The first starts from AVR = 1.05 along the back pressure increase. The second even covers the entire range around AVR = 1. Contrasting with Figure 13a, the reason for these divergences becomes rather straightforward. CFD can capture the impacts of rotation on secondary flows and, thus, loss mechanism, whereas correlations built upon cascade tests and calibrated to turbine data cannot. As a matter of fact, parameters or factors relating to rotation are absent in the correlations. In this view, reliability is globally guaranteed in stators and compromised in rotors because of rotation. Clearly, this observation constitutes the most sound argument against the use of cascades as benchmark of the correlations, as presented in the early review.

8. Conclusions

In this paper, historical insight was provided into the numerous features of the AM correlations, whose most authoritative contributions were given by AM, DC, KO, and Ag. These models were established empirically using measurements on turbine cascades and deliver a standardized solution for the configurations considered in the experiments. As a consequence, the range of applications of the models are biased towards the types of turbine cascades used to develop the correlations. An important restriction of the AM correlations is related to the profile loss, which is established through interpolation between nozzle and impulse blade empirical charts. This implies the prior setting of the velocity distribution over the blade surface, which follows from measurements on a restricted set of turbine cascade configurations. Another restriction is related to the secondary loss, which draws on the classical lifting-line theory of Carter and associates wingtip trailing vortices with blade passage vortices. Further investigation revealed a mathematical mistake in the secondary loss formulation and an undesirable link with the profile loss.

In light of these issues, an update to the profile and secondary losses was proposed in this work, building upon the correlations of Ag. For the profile loss, the addressed points are:

- The substitution of metal angle θ_{in} by the flow angle β_{in}.
- The scaling of the AM optimum pitch to chord s/c_{AM} by the Zweifel optimum pitch to chord s/c_Z. This, notably, preserves of the slope of the AM profile losses $Y_{p,\beta_{in}=0^\circ}$ and $Y_{p,\beta_{in}=-\beta_{out}}$ and adapts the AM correlation to other design rules.
- The use of a Reynolds number Re_s based on the suction surface length.
- The substitution of the auxiliary factor K_i by a more suitable incidence loss Y_{inc}, proposed by Benner et al.
- The reuse of the KO trailing edge loss $Y_{te,KO}$ affected by the profile loss auxiliary factors.

As for the secondary loss, the addressed points are:

- The replacement of the classical secondary flow model of AM and Carter by the endwall vortices model of Sharma and Butler.
- The use of the product of the elemental lift solidity coefficient $C_{L,out}/s/c$ and vortex penetration depth Z_{te} instead of the heuristic Ainley loading Z and parameter λ_{AM}.
- The invariance of the auxiliary factor K_{AR} beyond the threshold aspect ratio $H/c = 2$.
- The definition of a new auxiliary factor K_{sc}, to determine the variation of the secondary loss with the pitch to chord ratio s/c.

With a database of 109 cascades available, the prediction of the new correlation is benchmarked against the cascade numerical solution. Using descriptive statistics and expressing accuracy as the probability of achieving a relative error within ±15%, the improvement yields $\Delta P_{tol} = 45\%$ against the $\Delta P_{tol} = 22\%$ of Ag. Although there is a clear improvement, these results are largely dependent on the choice of a finite database for which the representativeness of the population is unknown. Nevertheless, this quantification should provide an estimate of the results and raise confidence in the use of the enhanced correlation. Regarding reliability, the new correlation ensures global consistency by reproducing the Smith chart [14] and off design stator loss variation. In addition, the analysis points out a correlation conservativeness in the design of the typical LPT, which is due to insensitivity to the secondary loss correlations beyond $H/c = 2$. Severe trend disruptions are identified during the application of the proposed enhanced correlation on four rotating cascades, the mismatches with CFD compromise its reliability in rotating flows.

Author Contributions: Conceptualization, Y.L.; methodology, Y.L.; software, Y.L.; validation, P.H. and Z.Z. and F.B.; formal analysis, Y.L.; investigation, Y.L.; resources, P.H. and Z.Z.; data curation, Y.L.; writing—original draft preparation, Y.L.; writing—review and editing, Y.L.; visualization, Y.L.; supervision, P.H. and Z.Z. and F.B.; project administration, P.H. and Z.Z.; funding acquisition, P.H. and Z.Z. All authors have read and agreed to the published version of the manuscript.

Funding: This research received no external funding.

Institutional Review Board Statement: Not applicable.

Informed Consent Statement: Not applicable.

Data Availability Statement: The cascade dataset and its CFD results are available on demand.

Conflicts of Interest: The authors declare no conflict of interest.

Nomenclature

Acronyms		
Ag	Aungier	
AM	Ainley and Mathieson	
BSM	Benner and Sjolander and Moustapha	
CFD	Computational fluid dynamics	
CFL	Courant–Friedrich–Levy	
DC	Dunham and Came	
E3	Energy efficient engine	
KO	Kacker and Okapuu	
LPT	Low pressure turbine	
MKT	Moustapha and Kacker and Tremblay	
VandV	Verification and validation	
Z	Zweifel	
Symbols		
β	Relative flow angle	[°]
$\Delta\Phi$	Kinetic loss coefficient	[-]
ΔP_{tol}	Tolerance interval probability	[-]
δ^*	Endwall displacement thickness	[m]
γ	Stagger	[°]
κ	Meanline radius ratio	[-]
λ_{AM}	Ainley parameter	[-]
ϕ	Flow coefficient	[-]
ψ	Blade loading	[-]
ψ_Z	Zweifel loading	[-]
σ	Standard deviation	[-]
θ	Metal angle	[°]
A	Cross section area	[m^2]
b	Axial chord	[m]
c	True chord	[m]
C_L	Lift coefficient	[-]
$C_{D,s}$	Secondary drag coefficient	[-]
d	Annulus diameter	[m]
d_{LE}	Leading edge diameter	[m]
E	Relative error	[-]
e	Surface roughness	[m]
e_c	Back curvature	[m^{-1}]

F_θ	Tangential loading	[-]
$f_{s/c}$	Scaling factor	[-]
H	Blade height	[m]
H'	Distance to endwall vortices	[m]
i	Incidence	[°]
K	Auxiliary factor	[-]
k	Heat ratio coefficient	[-]
K_{AR}	Aspect ratio correction	[-]
K_i	Incidence factor	[-]
K_{mod}	Technology factor	[-]
K_M	Expansion correction factor	[-]
K_m	Profile correction factor	[-]
K_p	Mach correction factor	[-]
K_{Re}	Reynolds correction factor	[-]
K_{sc}	Pitch to chord ratio correction	[-]
K_{te}	Trailing edge correction factor	[-]
M	Mach number	[-]
o	Throat width	[m]
p	Pressure	[Pa]
r	Meanline radius	[m]
Re	Reynolds number	[-]
Re_s	Suction length Reynolds number	[-]
s	Pitch	[m]
t_{max}	Maximum thickness	[m]
t_{te}	Trailing edge thickness	[m]
W	Relative velocity	[m/s]
We_{LE}	Leading edge wedge	[°]
Y_p	Profile loss	[-]
Y_s	Secondary loss coefficient	[-]
Y_t	Total loss coefficient	[-]
Y_{cl}	Tip clearance loss coefficient	[-]
Y_{ex}	Supersonic loss coefficient	[-]
Y_{inc}	Incidence loss coefficient	[-]
Y_{sh}	Shock factor	[-]
Y_{te}	Trailing edge loss coefficient	[-]
Z	Ainley loading	[-]
Z_{te}	Vortex penetration depth	[m]
AVR	Axial velocity ratio	[-]
CR	Convergence ratio	[-]
VR	Velocity ratio	[-]

Superscripts

$-$	Average

Subscripts

Enh	Enhanced
hub	Hub
in	Inlet
is	Isentropic
m	Mean
n	Normal
num	Numerical
out	Outlet
r	Relative
t	Total
tip	Tip
z	Axial

Appendix A

Table A1. Dimensionless parameters of the AM correlations.

Parameters	$Y_{p,AM}$	$Y_{s,AM}$	$Y_{p,Ag}$	$Y_{s,Ag}$	$Y_{te,Ag}$	$Y_{ex,Ag}$	Y_p	Y_s	Y_{te}
s/c	$\in$		$\in$				$\in$	$\in$	
t_{max}/c	$\in$		$\in$				$\in$		
θ_{in}	$\in$	$\in$	$\in$	$\in$			$\in$		
θ_{out}			$\in$				$\in$		
β_{in}		$\in$		$\in$				$\in$	$\in$
β_{out}	$\in$	$\in$	$\in$	$\in$			$\in$	$\in$	$\in$
t_{te}/s					$\in$				
o/s					$\in$				
e_c/s			$\in$				$\in$		
$M_{r,in}$			$\in$	$\in$			$\in$	$\in$	$\in$
$M_{r,out}$			$\in$	$\in$		$\in$	$\in$	$\in$	$\in$
Re			$\in$	$\in$					
Re_s							$\in$	$\in$	$\in$
e/c			$\in$	$\in$			$\in$	$\in$	$\in$
k			$\in$				$\in$		
i	$\in$		$\in$				$\in$		
d_{LE}/s							$\in$		
We_{LE}							$\in$		
A_{out}/A_{in}		$\in$							
r_{hub}/r_{tip}		$\in$							
H/c				$\in$				$\in$	
AVR							$\in$	$\in$	
ψ_Z							$\in$	$\in$	
t_{te}/o					$\in$				$\in$
δ^*/H								$\in$	
γ							$\in$	$\in$	
κ								$\in$	
Reference	Equation (2)	Equation (8)	Equation (3)	Equation (19)	Equation (7)	Equation (4)	Equation (20)	Equation (33)	Equation (24)
Total	5	5	12	8	3	1	17	13	7

References

1. Zou, Z.P.; Wang, S.T.; Liu, H.X.; Zhang, W.H. *Axial Turbine Aerodynamics for Aero-Engines: Flow Analysis and Aerodynamics Design*, 1st ed.; Springer Nature: Singapore, 2017.
2. Ainley, D.; Mathieson, G. *A Method for Performance Estimation for Axial-Flow Turbines*; Technical Report R&M No. 2974; Aeronautical Research Council: London, UK, 1951.
3. Dunham, J. 50 Years of Turbomachinery Research at Pyestock—Part 2: Turbines. *Aeronaut. J.* **2000**, *104*, 199–207. [CrossRef]
4. Dunham, J.; Came, P.M. Improvements to the Ainley-Mathieson Method of Turbine Performance Prediction. *J. Eng. Power* **1970**, *92*, 252–256. [CrossRef]
5. Kacker, S.C.; Okapuu, U. A Mean Line Prediction Method for Axial Flow Turbine Efficiency. *J. Eng. Power* **1982**, *104*, 111–119. [CrossRef]
6. Aungier, R. *Turbine Aerodynamics: Axial-Flow and Radial-Inflow Turbine Design and Analysis*; ASME Press: New York, NY, USA, 2006.
7. Japikse, D. *Turbomachinery Performance Modeling*; SAE Technical Paper 2009-01-0307; SAE: Beograd, Serbia, 2009. [CrossRef]
8. Lozza, G. A Comparison Between the Craig-Cox and the Kacker-Okapuu Methods of Turbine Performance Prediction. *Meccanica* **1982**, *17*, 211–221. [CrossRef]
9. Wei, N. Significance of Loss Models in Aerothermodynamic Simulation for Axial Turbines. Ph.D. Thesis, KTH Energiteknik, Stockholm, Sweden, 2000.
10. Coull, J.D.; Hodson, H.P. Blade Loading and Its Application in the Mean-Line Design of Low Pressure Turbines. *J. Turbomach.* **2013**, *135*, 12. [CrossRef]
11. Zweifel, O. Die Frage der optimalen Schaufelteilung bei Beschaufelungen von Turbomaschinen, insbesondere bei großer Umlenkung in den Schaufelreihen. *Brown Boveri Mitteilungen* **1945**, *32*, 436–444.
12. Sharma, O.P.; Butler, T.L. Predictions of Endwall Losses and Secondary Flows in Axial Flow Turbine Cascades. *J. Turbomach.* **1987**, *109*, 229–236. [CrossRef]
13. Benner, M.W.; Sjolander, S.A.; Moustapha, S.H. An Empirical Prediction Method for Secondary Losses in Turbines—Part I: A New Loss Breakdown Scheme and Penetration Depth Correlation. *J. Turbomach.* **2005**, *128*, 273–280. [CrossRef]
14. Smith, S. A Simple Correlation of Turbine Efficiency. *J. R. Aeronaut. Soc.* **1965**, *69*, 467–470. [CrossRef]
15. Moustapha, S.H.; Kacker, S.C.; Tremblay, B. An Improved Incidence Losses Prediction Method for Turbine Airfoils. *J. Turbomach.* **1990**, *112*, 267–276. [CrossRef]
16. Whittle, F. *Gas Turbine Aero-Thermodynamics: With Special Reference to Aircraft Propulsion*; Elsevier: Oxford, UK, 2013.
17. Craig, H.R.M.; Cox, H.J.A. Performance Estimation of Axial Flow Turbines. *Proc. Inst. Mech. Eng.* **1970**, *185*, 407–424. [CrossRef]

18. Dring, R.P.; Heiser, W.H. Turbine Aerodynamics. In *The Aerothermodynamics of Aircraft Gas Turbine Engines*; Oates, G.C., Ed.; NTIS: Seattle, WA, USA, 1978; Chapter 18; pp. 1–23.
19. Dunham, J. A Review of Cascade Data on Secondary Losses in Turbines. *J. Mech. Eng. Sci.* **1970**, *12*, 48–59. [CrossRef]
20. Denton, J. A Survey and Comparison of Methods for Predicting the Profile Loss of Turbine Blades. In Proceedings of the Conference on Heat and Fluid Flow in Steam and Gas Turbine Plant, Coventry, UK, 3–5 April 1973; Number RD/M/R143; pp. 204–212.
21. Chyu, M.K.; Young, G.M. *A Loss/Performance Evaluation of SSME HPFTP Turbine*; Technical Report NGT 01-002-099; NASA & University of Alabama: Huntsville, AL, USA, 1988.
22. Sieverding, C.H. Axial Turbine Performance Prediction Methods. In *Thermodynamics and Fluid Mechanics of Turbomachinery*; NATO ASI Series E; Kluwer Academic Publishers B.V.: Dordrecht, The Netherlands, 1985; Volume 1, pp. 737–784.
23. Liu, Y.M.; Hendrick, P.; Zou, Z.P.; Buysschaert, F. Statistical and Computational Evaluation of Empirical Axial Turbine Correlations in Design of Centrifugal Turbines. *J. Turbomach.* **2021**, *144*, 041002. [CrossRef]
24. Ainley, D.G. Performance of Axial-Flow Turbines. *Proc. Inst. Mech. Eng.* **1948**, *159*, 230–244. [CrossRef]
25. Traupel, W. *Thermische Turbomaschinen: Band 1: Thermodynamisch-Strömungstechnische Berechnung*; Springer: Berlin/Heidelberg, Germany, 2019.
26. Hirsch, C.; Denton, J.D. *Through Flow Calculations in Axial Turbomachines*; Technical Report AGARD-AR-175; Propulsion and Energetics Panel Working Group 12: Neuilly-sur-Seine, France, 1981.
27. Wu, C. *A General Theory of Three-Dimensional Flow in Subsonic and Supersonic Turbomachines in Radial and Mixed Flow Types*; Technical Report NACA TN-2604; National Advisory Committee for Aeronautics: Cleveland, OH, USA, 1952.
28. Da Lio, L.; Manente, G.; Lazzaretto, A. New efficiency charts for the optimum design of axial flow turbines for organic Rankine cycles. *Energy* **2014**, *77*, 447–459. [CrossRef]
29. Al Jubori, A.M.; Al-Dadah, R.K.; Mahmoud, S.; Daabo, A. Modelling and Parametric Analysis of Small-Scale Axial and Radial-Outflow Turbines for Organic Rankine Cycle Applications. *Appl. Energy* **2017**, *190*, 981–996. [CrossRef]
30. Baljé, O.E.; Binsley, R.L. Axial Turbine Performance Evaluation. Part A—Loss-Geometry Relationships. *J. Eng. Power* **1968**, *90*, 341–348. [CrossRef]
31. Denton, J.D. The 1993 IGTI Scholar Lecture: Loss Mechanisms in Turbomachines. *J. Turbomach.* **1993**, *115*, 621–656. [CrossRef]
32. Coull, J.D.; Hodson, H.P. Predicting the Profile Loss of High-Lift Low Pressure Turbines. *J. Turbomach.* **2012**, *134*, 14. [CrossRef]
33. Ainley, D. *An Approximate Method for the Estimation of the Design Point Efficiency of Axial Flow Turbines*; Technical Report R&M No. 59; Aeronautical Research Council: London, UK, 1950.
34. Ainley, D.; Mathieson, G. *An Examination of the Flow and Pressure Losses in Blade Rows of Axial Flow Turbines*; Technical Report R&M No. 2891; Aeronautical Research Council: London, UK, 1951.
35. Carter, A.D.S. Three-Dimensional-Flow Theories for Axial Compressors and Turbines. *Proc. Inst. Mech. Eng.* **1948**, *159*, 255–268. [CrossRef]
36. Lakshminarayana, B.; Horlock, J.H. Review: Secondary Flows and Losses in Cascades and Axial-Flow Turbomachines. *Int. J. Mech. Sci.* **1963**, *5*, 287–307. [CrossRef]
37. Zhu, J.; Sjolander, S.A. Improved Profile Loss and Deviation Correlations for Axial-Turbine Blade Rows. Turbo Expo 2005, Parts A and B. In *Turbo Expo: Power for Land, Sea, and Air*; ASME Paper No. GT2005-69077; ASME: Reno, NV, USA, 2005; Volume 6, pp. 783–792. [CrossRef]
38. Dunham, J. Loss Mechanisms and Unsteady Flows in Turbomachines. In Proceedings of the Technical Report AGARD-CP-571, Propulsion and Energetics Panel 85th Symposium, Derby, UK, 8–12 May 1995.
39. Stabe, R.G.; Kline, J.F. *Incidence Loss for a Core Turbine Rotor Blade in a Two-Dimensional Cascade*; Technical Report NASA TM X-3047; NASA: Washington, DC, USA, 1974.
40. Hawthrone, W.R. *Aerodynamics of Turbines and Compressors*; *High Speed Aerodynamics and Jet Propulsion*; Princeton University Press: Princeton, NJ, USA, 1964; Volume 10.
41. Perdichizzi, A.; Dossena, V. Incidence Angle and Pitch–Chord Effects on Secondary Flows Downstream of a Turbine Cascade. *J. Turbomach.* **1993**, *115*, 383–391. [CrossRef]
42. Teia, L. New Insight Into Aspect Ratio's Effect on Secondary Losses of Turbine Blades. *J. Turbomach.* **2019**, *141*. [CrossRef]
43. Walsh, J.A.; Gregory-Smith, D.G. Inlet Skew and the Growth of Secondary Losses and Vorticity in a Turbine Cascade. *J. Turbomach.* **1990**, *112*, 633–642. [CrossRef]
44. Agromayor, R.; Nord, L.O. Preliminary Design and Optimization of Axial Turbines Accounting for Diffuser Performance. *Int. J. Turbomach. Propuls. Power* **2019**, *4*, 32. [CrossRef]
45. Tournier, J.M.; El-Genk, M.S. Axial Flow, Multi-Stage Turbine and Compressor Models. *Energy Convers. Manag.* **2010**, *51*, 16–29. [CrossRef]
46. Korpela, S.A. *Principles of Turbomachinery*, 2nd ed.; John Wiley & Sons: Hoboken, NJ, USA, 2020.
47. Concepts/ETI. *Loss Models In Axial (Reduced Throughflow) and AxCent (NS Throughflow) Solvers*; Concepts NREC: White River Junction, VT, USA, 2014.
48. Benner, M.W.; Sjolander, S.A.; Moustapha, S.H. Influence of Leading-Edge Geometry on Profile Losses in Turbines at Off-Design Incidence: Experimental Results and an Improved Correlation. *J. Turbomach.* **1997**, *119*, 193–200. [CrossRef]

49. Brown, L.E. Axial Flow Compressor and Turbine Loss Coefficients: A Comparison of Several Parameters. *J. Eng. Power* **1972**, *94*, 193–201. [CrossRef]
50. Sieverding, C.; Manna, M. A Review on Turbine Trailing Edge Flow. *Int. J. Turbomach. Propuls. Power* **2020**, *5*, 10. [CrossRef]
51. Lewis, R.I. *Turbomachinery Performance Analysis*; Butterworth-Heinemann: Oxford, UK, 1996.
52. Kraft, H. Reaction Tests of Turbine Nozzles for Subsonic Velocities. *Trans. ASME* **1949**, *71*, 781–787.
53. Hodson, H.P.; Dominy, R.G. The Off-Design Performance of a Low-Pressure Turbine Cascade. *J. Turbomach.* **1987**, *109*, 201–209. [CrossRef]
54. Benner, M.W.; Sjolander, S.A.; Moustapha, S.H. An Empirical Prediction Method For Secondary Losses In Turbines—Part II: A New Secondary Loss Correlation. *J. Turbomach.* **2005**, *128*, 281–291. [CrossRef]
55. Yaras, M.I.; Sjolander, S.A. Prediction of Tip-Leakage Losses in Axial Turbines. *J. Turbomach.* **1992**, *114*, 204–210. [CrossRef]
56. Farokhi, S. Analysis of Rotor Tip Clearance Loss in Axial-Flow Turbines. *J. Propuls. Power* **1988**, *4*, 452–457. [CrossRef]
57. Denton, J.D. Some Limitations of Turbomachinery CFD. Turbomachinery, Parts A, B, and C. In Proceedings of the ASME Turbo Expo 2010: Power for Land, Sea, and Air, Glasgow, UK, 14–18 June 2010; Volume 7, pp. 735–745. [CrossRef]
58. Oberkampf, W.L.; Blottner, F.G. Issues in Computational Fluid Dynamics Code Verification and Validation. *AIAA J.* **1998**, *36*, 687–695. [CrossRef]
59. Stern, F.; Wilson, R.V.; Coleman, H.W.; Paterson, E.G. Comprehensive Approach to Verification and Validation of CFD Simulations—Part 1: Methodology and Procedures. *J. Fluids Eng.* **2001**, *123*, 793–802. [CrossRef]
60. Walraevens, R.; Gallus, H. *Test Case 6: 1—1/2 Stage Axial Flow Turbine*; Technical Report, ERCOFTAC SIG on 3D Turbomachinery Flow Prediction; ERCOFTAC Turbomachinery Seminar and Workshop: Les Arcs, France, 1997.
61. Cadence/NUMECA. *FINE/Turbo 16.1 Theory Guide*; Cadence/NUMECA: Brussels, Belgium, 2021.
62. Menter, F.R.; Garbaruk, A.V.; Egorov, Y. Explicit Algebraic Reynolds Stress Models for Anisotropic Wall-Bounded Flows. *Prog. Flight Phys.* **2012**, *3*, 89–104. [CrossRef]
63. Mendenhall, W.; Beaver, R.J.; Beaver, B.M. *Introduction to Probability and Statistics*; Cengage Learning: Boston, MA, USA, 2012.
64. Horlock, J.H. *Axial Flow Turbines: Fluid Mechanics and Thermodynamics*; Butterworths: London, UK, 1973.
65. Cherry, D.; Gay, C.; Lenahan, D. *Energy Efficient Engine Low Pressure Turbine Test Hardware Detailed Design Report*; Technical Report NASA-CR-167956; General Electric Company: Washington, DC, USA, 1984.
66. Leach, K.; Thulin, R.; Howe, D. *Energy Efficient Engine: Turbine Intermediate Case and Low-Pressure Turbine Component Test Hardware Detailed Design Report*; Technical Report NASA-CR-167973; United Technologies Corporation: Washington, DC, USA, 1984.